

Change point analysis of high-dimensional data using random projections

YI XU AND YEONWOO RHO¹

Department of Mathematical Sciences, Michigan Technological University

March 4, 2026

Abstract

This paper develops a novel change point identification method for high-dimensional data using random projections. By projecting high-dimensional time series into a one-dimensional space, we are able to leverage the rich literature for univariate time series. We propose applying random projections multiple times and then combining the univariate test results using existing multiple comparison methods. Simulation results suggest that the proposed method tends to have better size and power, with more accurate location estimation. At the same time, random projections may introduce variability in the estimated locations. To enhance stability in practice, we recommend repeating the procedure, and using the mode of the estimated locations as a guide for the final change point estimate. An application to an Australian temperature dataset is presented. This study, though limited to the single change point setting, demonstrates the usefulness of random projections in change point analysis.

Keywords— Change point analysis; High-dimensional data; Random projections; CUSUM; p-value combination method

1 Introduction

Change point detection plays a crucial role in science by identifying shifts in the underlying dynamics of a system. While change point analysis has been extensively studied in low-dimensional settings (e.g., Csörgö and Horváth (1997); Aue and Horváth (2013); Horváth and Rice (2014); Aminikhanghahi and Cook (2017)), modern applications increasingly generate high-dimensional vectors or functional observations. Examples arise in neuroscience through functional magnetic resonance imaging (Aston and Kirch, 2012b), in finance via panels of S&P500 stock prices (Horváth et al., 2014; Jirak, 2015), and in climate studies through long term temperature trajectories (Aue et al., 2018). Detecting the precise timing of dynamic shifts in such high-dimensional or functional data has increasingly attracted attention in the literature.

¹Author of Correspondence: Y. Rho (yrho@mtu.edu)

Current change point detection methods for high-dimensional or functional data can be broadly divided into three categories: projection-based, fully functional, and manipulations of multivariate statistics. Projection-based approaches involve some form of dimension reduction and rely on classical univariate change point tools, such as cumulative sum (CUSUM) tests (Page, 1954, 1955). For instance, functional principal component (FPC) analysis projects the high-dimensional or functional data onto a few leading directions that capture the majority of variance (Berkes et al., 2009; Aue et al., 2009; Aston and Kirch, 2012a). Wang and Samworth (2018) seeks a single projection direction that aligns the most with the change. The CUSUM-type statistics are applied to the projected data afterwards. While these approaches leverage well-established univariate tools, reducing the data to one or a few dimensions may lose information if the projection does not fully capture the structure of the change. For instance, the FPC-based technique cannot consistently detect the change if the mean break function is orthogonal to the direction of FPCs (Aue et al., 2018). Fully-functional methods (Horváth et al., 2014; Aue et al., 2018; Dette et al., 2020) are relatively free of such projection-induced limitations. However, they assume the underlying signal is sufficiently smooth, which may limit their applicability to certain types of data. These methods require a smoothing step since observations are often only on discrete grids, and improper smoothing can negatively affect results. For example, using too few basis functions for densely observed data may remove high-frequency variations (Jiao et al., 2022), while using too many basis functions can produce excessively large covariance matrices, leading to slow computation. The last category is based on multivariate statistics, often in a CUSUM form, which are then aggregated using suitable norms or other manipulations (Bai, 2010; Horváth and Hušková, 2012; Chan et al., 2013; Jirak, 2015; Cho, 2016; Enikeeva and Harchaoui, 2019; Liu et al., 2020; Yu and Chen, 2021; Wang et al., 2022; Wang and Feng, 2023). See Liu et al. (2022) for an extensive review of existing change point detection methods in high-dimensional vector settings. The method proposed in this paper can be viewed as a combination of the projection-based method and the last category. Our method also aggregates a multivariate CUSUM statistic, but unlike existing methods, this statistic is constructed from projections rather than the original high-dimensional vectors.

In this paper, we employ random projections. Random projection is a popular dimension-reduction tool (Bingham and Mannila, 2001; Dasgupta, 2000). While Aston and Kirch (2018) consider a random projection in the context of change point detection for high-dimensional data, only one random projection is considered, which is proposed as the lower benchmark when measuring efficiency of change point detection methods. However, one random projection is unlikely to capture the underlying structure of the original space unless multiple projections are involved. To address this limitation, our method aggregates across multiple random projections. An ensemble of many random projections and proper aggregation captures the change in the original dimension, avoiding the possible loss of information that is common in other projection-based

approaches. Our method does not suffer from the limitations of the fully functional approaches, without requiring either the smoothness assumption nor the basis functions. By relying on projections, our method avoids complications associated with other multivariate CUSUM statistics: the covariance matrix of the multivariate CUSUM statistic does not need to be estimated, nor are tools such as self-normalization or bootstrapping required, and no assumption of independence across dimensions is needed. Our approach may not fully exploit the dimensionality reduction property of random projections, as current theoretical guarantees ensure that information in the original data can be preserved only when the number of projections is equal to or greater than the original dimension (Lee et al., 2005; Ghojogh et al., 2021). Nevertheless, we will demonstrate that random projections still provide a valuable framework for change analysis.

Adapting random projections to change point analysis involves many choices: projection directions and their number, the univariate change point tests, and the aggregation procedure. A guideline of such choices is provided through extensive simulations, where size and power of global tests as well as accuracy of location estimates are explored. For the univariate change point tests, CUSUM tests and its variants are considered in our simulations. Aggregation methods include the classical approaches, such as Bonferroni’s correction (Bonferroni, 1936) and Benjamini–Hochberg procedure (Benjamini and Hochberg, 1995), as well as more recently proposed p -value combination techniques such as harmonic mean p (Wilson, 2019) and Cauchy combination tests (Liu and Xie, 2020). In addition, random projections may introduce high variability in the location estimation. We propose to repeat the random projection-CUSUM-aggregation procedure multiple times for stability.

The advantages of the proposed method can be summarized as follows. First, using random projections, our method is easy to implement, taking advantage of the rich literature and computational ease of univariate time series. Second, compared to other projection-based methods, which heavily rely on the quality of selected directions, our method eliminates the need for exploration of optimal projection direction and the possible information loss due to dimension reduction. Third, our method does not rely on the functional framework, which requires smooth functions.

The remainder of the paper is organized as follows. We introduce the proposed method in Section 2. Section 3 presents simulation results: parameter choices are discussed in Subsection 3.1, and comparison with other existing methods are presented in Subsection 3.2. Subsection 3.3 demonstrates the ability to correctly capture change locations despite the variability introduced by random projections, when our method is repeatedly applied. Section 4 illustrates the applications to an Australian temperature data. Section 5 is the conclusion.

2 Random projection change point detection method

Let $\mathbf{x}_t = (X_{t1}, \dots, X_{tp})^T$ be a p -dimensional time series. Our interest is to detect a change point in the mean vectors such that $E(\mathbf{x}_1) = E(\mathbf{x}_2) = \dots = E(\mathbf{x}_{z^*}) \neq E(\mathbf{x}_{z^*+1}) = \dots = E(\mathbf{x}_n)$, where z^* denotes a possible (unknown) change point location, and $z^* = \lfloor \theta n \rfloor$, $\theta \in (0, 1)$. The time series $\mathbf{x}_1, \dots, \mathbf{x}_n$ are modeled by:

$$\mathbf{x}_t = \boldsymbol{\mu} + \boldsymbol{\delta} \mathbb{1}\{t > z^*\} + \boldsymbol{\varepsilon}_t, \quad 1 \leq t \leq n, \quad (2.1)$$

where $\boldsymbol{\mu} \in \mathbb{R}^p$ is a baseline mean vector, $\boldsymbol{\delta} \in \mathbb{R}^p$ is the change in the mean vector after z^* . We denote \mathbb{R}^p as a space of p -dimensional vectors of real numbers. $\mathbb{1}\{t > z^*\}$ is an indicator function which maps t to one if $t > z^*$ and to zero if $t \leq z^*$. We are interested in a hypothesis testing regarding the break vector $\boldsymbol{\delta}$:

$$H_0 : \boldsymbol{\delta} = \mathbf{0} \quad \text{versus} \quad H_A : \boldsymbol{\delta} \neq \mathbf{0}. \quad (2.2)$$

For the p -dimensional errors $\boldsymbol{\varepsilon}_t = (\varepsilon_{t1}, \dots, \varepsilon_{tp})^T$, any weak stationarity assumption would work. Here, we present the linear process assumption, following [Aston and Kirch \(2018\)](#), where the random behaviors of a randomly projected time series is explored:

Assumption 2.1 (Linear process). *The error sequence $\boldsymbol{\varepsilon}_t = (\varepsilon_{t1}, \dots, \varepsilon_{tp})^T$ is a linear process of the form*

$$\boldsymbol{\varepsilon}_t = \sum_{l=0}^{\infty} \boldsymbol{\psi}_l e_{t-l},$$

where $\{e_t\}_{t \in \mathbb{Z}}$ is an independent and identically distributed (i.i.d.) sequence with $\mathbb{E}(e_t) = 0$, $\text{Var}(e_t) = 1$ and $\mathbb{E}(|e_t|^{2+\delta}) < \infty$ for some $\delta > 0$. The coefficients $\boldsymbol{\psi}_l = (\psi_{1,l}, \dots, \psi_{p,l})^T$ satisfy

$$\sum_{l=0}^{\infty} \psi_{j,l}^2 < \infty, \quad j = 1, \dots, p.$$

Our method is organized into two steps, the random projections (RP) step and the univariate change point tests (CUSUM) and their combination step, as outlined below.

2.1 Step 1: RP Step

The first step is to apply RP to a p -dimensional time series $X = (\mathbf{x}_1, \dots, \mathbf{x}_n)^T \in \mathbb{R}^{n \times p}$ to obtain k univariate time series $Y = \frac{1}{\sqrt{k}}XD = (\mathbf{y}_1, \dots, \mathbf{y}_k) \in \mathbb{R}^{n \times k}$, where $D = (\mathbf{d}_1, \dots, \mathbf{d}_k) \in \mathbb{R}^{p \times k}$ contains the k random directions. Here, the r^{th} direction is denoted by $\mathbf{d}_r = (d_{1,r}, \dots, d_{p,r})^T \in \mathbb{R}^p$, $1 \leq r \leq k$, and the r^{th} projected time series by $\mathbf{y}_r = (y_{1,r}, \dots, y_{n,r})^T \in \mathbb{R}^n$, where $y_{t,r} = \frac{1}{\sqrt{k}}\mathbf{x}_t^T \mathbf{d}_r$, $1 \leq t \leq n$. The RP preserves pairwise

Algorithm 1 RP method for a single mean change point detection

Input: Original data: $X \in \mathbb{R}^{n \times p}$,

Number of random projections: k ,

Output: Estimated change point location: $\hat{z}^* \in [1, n]$,

Combined p -value: p_{comb} .

Steps:

1. [RP] Perform random projections $Y = XD = (\mathbf{y}_1, \dots, \mathbf{y}_k) \in \mathbb{R}^{n \times k}$, where elements of D are drawn from distribution (2.3).

2. [CUSUM and Combination] Apply a univariate CUSUM test to $\mathbf{y}_r = (y_{1,r}, \dots, y_{n,r})^T$, $1 \leq r \leq k$. Compute the adjusted p -values $p_{adj(r)}$, and the combined p -value $p_{comb} = \min_{1 \leq r \leq k} p_{adj(r)}$.

Let $\hat{z}^* = \arg \max_{\lfloor n\tau \rfloor \leq z \leq n - \lfloor n\tau \rfloor} T_{z, \tilde{r}}$ in equation (2.5), where $\tilde{r} = \arg \min_{1 \leq r \leq k} p_{adj(r)}$.

distance to certain accuracy (Johnson and Lindenstrauss, 1984; Arriaga and Vempala, 1999). Intuitively, the projected time series also preserve useful information about the mean change and the stationarity of the original time series if $\boldsymbol{\delta}^T \mathbf{d}_r \neq \mathbf{0}$ because

$$E(y_{t,r} | \mathbf{d}_r) = E\left(\frac{1}{\sqrt{k}} \mathbf{x}_t^T \mathbf{d}_r | \mathbf{d}_r\right) = \frac{1}{\sqrt{k}} E(\mathbf{x}_t^T) \mathbf{d}_r = \begin{cases} \frac{1}{\sqrt{k}} \boldsymbol{\mu}^T \mathbf{d}_r, & t \leq z^*, \\ \frac{1}{\sqrt{k}} (\boldsymbol{\mu} + \boldsymbol{\delta})^T \mathbf{d}_r, & t > z^*. \end{cases}$$

There are two choices to make in this first step: the way to generate random directions and the number of projections. For the random directions, several approaches have been proposed to generate the entries $d_{j,r}$ for $1 \leq j \leq p$, $1 \leq r \leq k$ in the direction matrix D . Arriaga and Vempala (1999) propose two methods. One option is selecting the entries $d_{j,r}$ independently from a standard normal distribution. Another option is selecting elements independently from a discrete distribution, where $d_{j,r} = 1$ with probability $\frac{1}{2}$ and $d_{j,r} = -1$ with probability $\frac{1}{2}$. In fact, Arriaga and Vempala (1999) prove that the elements $d_{j,r}$ can be drawn independently from any distribution with a mean of zero and a bounded fourth moment. Achlioptas (2003) argues that having sparse \mathbf{d} is also acceptable, proposing “sparse random projections,” where the entries $d_{j,r}$ are independent random variables following a probability distribution:

$$d_{j,r} = \sqrt{3} \begin{cases} 1 & \text{with probability } 1/6, \\ 0 & \text{with probability } 2/3, \\ -1 & \text{with probability } 1/6. \end{cases} \quad (2.3)$$

As Achlioptas (2003) explains, a “threefold speedup” can be achieved using this sparse \mathbf{d} , which randomly drops approximately two-thirds of the original data. To further reduce computational cost, Li et al. (2006) propose “very sparse random projections” which requires only $1/b$ of the original data to be processed, where $b \in \mathbb{Z}$ and $b \gg 3$. While a larger b speeds the computation up significantly, Li et al. (2006) notice that

higher sparsity increases the variance of the pairwise distances of projected data, pointing out that using $b < 3$ can achieve smaller variability than a large b . In our approach, we follow [Achlioptas \(2003\)](#), setting $b = 3$, to balance between computational cost and stability. For the number of projections, a theoretical bound is provided in the Johnson-Lindenstrauss (JL) lemma ([Johnson and Lindenstrauss \(1984\)](#)), which aims to preserve pairwise distances. However, [Bingham and Mannila \(2001\)](#) achieve satisfactory empirical performance using far fewer projections than the JL bound suggests. Our simulation results in Subsection [3.1](#) with sample size $n = 50$ also reveal that using a relatively small number of projections, $k = 200$, can already achieve high accuracy. The larger the signal-to-noise ratio is, the smaller the number of random projections is needed.

2.2 Step 2: CUSUM and Combination Step

The second step is to apply an existing univariate change point test on each projected time series $\mathbf{y}_r = (y_{1,r}, \dots, y_{n,r})^T$, $r = 1, \dots, k$, and then combine the k tests with a p -value combination method. There are two choices to make in the second step: the type of univariate change point test and the type of p -value combination method.

We first discuss the type of univariate change point test. Theorem 3.1 of [Aston and Kirch \(2018\)](#) proves that, given a random direction \mathbf{d}_r independent of $\{\varepsilon_t : 1 \leq t \leq n\}$, under Assumption [2.1](#) and H_0 ,

$$\left\{ \frac{\mathcal{Z}_{n,r}(x)}{\hat{\sigma}} : 0 \leq x \leq 1 | \mathbf{d}_r \right\} \xrightarrow{D[0,1]} \left\{ B(x) : 0 \leq x \leq 1 \right\} \quad a.s.,$$

where $\mathcal{Z}_{n,r}(x) = \frac{1}{\sqrt{n}} \left| \sum_{t=1}^{\lfloor nx \rfloor} y_{t,r} - \frac{\lfloor nx \rfloor}{n} \sum_{t=1}^n y_{t,r} \right|$, $\hat{\sigma}$ is a consistent estimator of the long-run variance of the projected series, and $B(x)$ is a standard Brownian bridge. This theorem justifies the use of classical change point detection methods for univariate time series, such as the standard cumulative sum (CUSUM) test ([Page, 1954](#)) and its variants, to the RP-projected data. A weighted version of the CUSUM ([Csörgö and Horváth, 1993, 1997](#)) applies a weight function to stabilize the variance, often attaining higher power in detecting early or late change points as explained in [Aue and Horváth \(2013\)](#). Other CUSUM-based tests can also be considered, we refer readers to reviews in [Aue and Horváth \(2013\)](#) and [Horváth and Rice \(2014\)](#). Our simulations in Subsection [3.1](#) suggests that the standard or weighted CUSUM perform the best, when combined with RP, in terms of size and power. We write the standard and weighted CUSUM statistics as $T_{z,r}^s = \frac{1}{\hat{\sigma}_z} \mathcal{Z}_{n,r} \left(\frac{z}{n} \right)$ and

$$T_{z,r}^w = \frac{1}{\hat{\sigma}_z \sqrt{n}} \left(\frac{z(n-z)}{n^2} \right)^{-\frac{1}{2}} \left| \sum_{t=1}^z y_{t,r} - \frac{z}{n} \sum_{t=1}^n y_{t,r} \right| = \frac{1}{\hat{\sigma}_z} \sqrt{\frac{n}{z(n-z)}} \left| \sum_{t=1}^z y_{t,r} - \frac{z}{n} \sum_{t=1}^n y_{t,r} \right|, \quad (2.4)$$

respectively. The details on $\hat{\sigma}_z$ will be discussed in Subsection 3.1. In what follows, $T_{z,r}$ shall denote either $T_{z,r}^s$ or $T_{z,r}^w$.

For the p -value combination method, two classical methods are illustrated here: the Bonferroni (Bonf) (Bonferroni, 1936) and Benjamini and Hochberg (1995) (BH) methods. Denote p_r , $r = 1, \dots, k$, by the p -values of the univariate change point tests of the projected data, and $p_{(1)}, \dots, p_{(k)}$ by their ordered version from smallest to largest. The Bonferroni- and BH-adjusted p -values are $p_{adj(r)}^{Bonf} = kp_r$, and $p_{adj(r)}^{BH} = \min\{1, \min_{r \leq h \leq k} \{\frac{kp_{(h)}}{h}\}\}$, respectively. The global null is rejected when $p_{adj(r)}$ is less than the significance level.

While other p -value combination methods can also be considered, such as Wilson (2019); Liu and Xie (2020), but the advantage of Bonf and BH is that the identification of significant test is straightforward. Change locations are identified as follows. We first identify the projected data that leads to the largest change, or equivalently, smallest adjusted p -value: $\tilde{r} = \arg \min_{1 \leq r \leq k} p_{adj(r)}$. The change location is estimated as

$$\hat{z}^* = \arg \max_{\lfloor n\tau \rfloor \leq z \leq n - \lfloor n\tau \rfloor} T_{z, \tilde{r}}, \quad (2.5)$$

where $\tau \in (0, \frac{1}{2})$ is a trimming parameter for the weighted CUSUM. We set $\tau = 1/n$ for the standard CUSUM.

The validity of this location estimate is anchored through the RP's ability to capture the pairwise distance (Lee et al., 2005), even with the L_∞ norm, as long as the number k of projections is large. Recall that under the null, the random behavior of a projected data \mathbf{y}_r using a random projection is similar to that of a component of the high-dimensional data (Theorem 3.1 of Aston and Kirch (2018)). When \tilde{r} is chosen with $p_{adj(r)}^{Bonf}$, Yu and Chen (2021) provide the rate of convergence of \hat{z}^* to the true change location z^* when weighted CUSUM $T_{z,r}^w$ (Theorem 3.4) or standard CUSUM $T_{z,r}^s$ (Theorem 3.5) is used.

3 Simulation

This simulation section has three goals. We first provide a guide on the parameter choices involved in our method through extensive simulations in Subsection 3.1, and identify reasonable RP-CUSUM procedures. Comparisons of our RP-CUSUM with other change point methods for high-dimension or functional data follow in Subsection 3.2. Subsection 3.3 demonstrates that while RP-CUSUM may exhibit variability in a single run, it tends to correctly identify the change location with repetitions.

In the simulations in this section, data are generated similarly to the functional setting described in Aue et al. (2018). We first formulate our change point model presented in (2.1) in a functional framework:

$X_t(\frac{j}{p}) = X_{tj}$, $j = 1, \dots, p$, where X_1, \dots, X_n denote functional time series on a unit interval $[0, 1]$. A single change point model for the functional time series is

$$X_t(s) = \mu(s) + \delta(s)\mathbb{1}\{t > z^*\} + \varepsilon_t(s), \quad 1 \leq t \leq n, \quad s \in [0, 1], \quad (3.1)$$

where μ , δ , and ε_t are functions defined on the unit interval $[0, 1]$. Let $\mu(s) = 0$ and

$$\varepsilon_t(s) = \sum_{g=1}^D A_{t,g} v_g(s), \quad 1 \leq t \leq n, \quad s \in [0, 1], \quad (3.2)$$

with Fourier basis functions $v_1(s), \dots, v_D(s)$. The basis coefficients $A_{t,g}$ are drawn independently from a normal distribution with mean zero and standard deviation σ_g of the following three settings:

Setting 1: $\sigma_g = 1$ for $g = 1, 2, 3$ and $\sigma_g = 0$ for $g = 4, \dots, D$.

Setting 2: $\sigma_g = 3^{-g}$ for $g = 1, \dots, D$.

Setting 3: $\sigma_g = g^{-1}$ for $g = 1, \dots, D$.

The three settings of σ_g model different forms in the decay of the ordered eigenvalues of the covariance matrix in the functional data setting. *Setting 1* concerns the situation that only three basis functions are included in the functional data. *Setting 2* involves the situation in which the eigenvalues of the covariance matrix decay fast, while *Setting 3* relates to the situation in which the eigenvalues decay slowly.

When the eigenvalues of the covariance matrix decay faster, fewer eigenfunctions are needed to explain most of the variation in the functional data samples. Specifically, in *Setting 1*, the majority of variation is explained by the first three eigenfunctions, with each contributing relatively evenly. In *Setting 2*, the first two eigenfunctions tend to explain about 95% of total variation, with the first eigenfunction explaining much more than the second eigenfunction. In *Setting 3*, the proportion of variation explained by eigenfunctions decreases gradually, requiring more than three eigenfunctions to capture most of the variation.

The break function $\delta(s)$ in model (3.1) is formulated with the first m basis functions $v_1(s), \dots, v_m(s)$, where $m \leq D$. The magnitude of the break function is scaled by the signal-to-noise ratio (*SNR*) as follows:

$$\delta(s) = \delta(s; m, c) = \sqrt{c} * \frac{1}{\sqrt{m}} \sum_{g=1}^m v_g(s), \quad c = \text{SNR} * \frac{\text{tr}(C_\varepsilon)}{\theta(1-\theta)\sqrt{D}}, \quad (3.3)$$

where θ is the scaled location of the change point in the interval $(0, 1)$, and C_ε is the long-run variance of the errors. Note that $m = 1$ corresponds to a constant mean break. When $m > 1$, the break is spread over a larger number of basis functions, resulting in a more complex form. Following the simulation codes from

Aue et al. (2018), the term $tr(C_\varepsilon)$ is computed as the trace of the sample covariance matrix for the centered basis coefficients $A_{t,g}$ of the functional errors.

Following Aue et al. (2018)'s setting, $D = 21$ and $n = 50$. The values of SNR are 0, 0.1, 0.2, 0.3, 0.5, 1, and 1.5, with $SNR = 0$ indicating $\delta(s) = 0$ (H_0), while $SNR > 0$ represent alternative cases. The break function $\delta(s)$ is constructed with $m = 1, 5, \text{ or } 20$. When discretization of the functional data is needed for our RP methods or for the method in Wang and Samworth (2018), we evaluate functions at equally spaced grid points $\frac{j}{p} \in [0, 1]$, $j = 1, \dots, p$, with $p = 101$. All results are based on 1000 simulations unless otherwise specified.

3.1 Parameter Choices for the RP method

Our RP methods require three choices: the types of change point tests, p -value combination methods, and the number of random projections. In this subsection, we provide an empirical guide on such choices through simulations.

For the change point tests, there is extensive literature on detecting and locating change points. Horváth and Rice (2014) provide a survey of some widely used change point methods. For those applicable to univariate time series, they include the standard CUSUM test (Page, 1954), the weighted CUSUM (Csörgő and Horváth, 1993, 1997), Darling-Erdős (DE) test (Darling and Erdős, 1956), Andrews test (Andrews, 1993), and Hidalgo and Seo (HS) test (Hidalgo and Seo, 2013). Furthermore, Horváth et al. (2020) compare the above tests with their newly developed Rényi-type (HR) test, and mention that the Andrews test statistics have a similar performance to that of the DE test. Our simulation focuses on five tests: the standard CUSUM, the weighted CUSUM, DE, HS, and HR tests.

When implementing the weighted CUSUM test, the change point estimation in (2.5) is restricted to the trimmed interval $[\lfloor n\tau \rfloor, n - \lfloor n\tau \rfloor]$, where $\tau \in (0, \frac{1}{2})$. We consider choices of $\lfloor n\tau \rfloor$ including 1, $\lfloor n^{0.25} \rfloor, \lfloor \log(n) \rfloor, \lfloor n^{0.5} \rfloor$ following Horváth et al. (2020). To simulate the limiting distribution of the weighted CUSUM, we generate 100,000 replications and use 10,000 increments for Brownian bridge. When estimating σ_z^2 in (2.4), we consider the heteroskedasticity and autocorrelation consistent (HAC) estimation with the Bartlett kernel and the bandwidth based on Andrews (1991). Alternative combinations of kernel function and bandwidth are also compared but leads to inferior results, which are not presented. We also consider a variance estimator as mentioned in Horváth et al. (2020). Using y_t to represent $y_{t,r}$ for simplicity, for any $r = 1, \dots, k$, $\hat{\sigma}_z^2 = \frac{1}{n} [(\sum_{t=1}^z (y_t - \bar{y}_z)^2 + \sum_{t=z+1}^n (y_t - \bar{y}_{n-z})^2)]$, where $\bar{y}_z = \frac{1}{z} \sum_{t=1}^z y_t$, and $\bar{y}_{n-z} = \frac{1}{n-z} \sum_{t=z+1}^n y_t$. The overall conclusions of comparison using this variance estimator remain consistent with those using the HAC estimator. When the time series is known to be uncorrelated, the variance estimators $\hat{\sigma}_z^2$ from Horváth et al.

(2020) is recommended as it is computationally faster than the HAC estimators. We present the results using the variance estimator from Horváth et al. (2020) in the main paper, and the results obtained using the HAC estimator in the Supplementary Material S.1.1.

For the p -value combination methods, there are a variety of approaches that control the family-wise error rate (FWER) or false discovery rate (FDR) among multiple tests. In addition to the Bonf and BH methods, mentioned in Subsection 2.2, we also consider the Cauchy combination test (CCT) from Liu and Xie (2020) and the Harmonic mean p -value (HMP) (Wilson, 2019) for a better FWER control and improved power when tests are dependent. The Benjamini-Yekutieli (BY) method (Benjamini and Yekutieli, 2001), an extension of BH method to handle dependent tests, is also considered but not presented since the BH method has better performance than the BY method when combined with random projections based on our simulation results. We further use BH and Bonf methods for change point location identification based on the smallest adjusted p -value.

For the number k of random projections, a theoretical bound from Dasgupta and Gupta (2003) is $4(a^2/2 - a^3/3)^{-1} \ln n$, where $0 < a < 1$ and $(1 - a)$ relates to the accuracy of random projections in preserving pairwise distances. This bound suggests that approximately 900 projections are required for the data settings we consider, with $a = 0.2$ and $n = 50$. Given this theoretical bound and the empirical findings from Bingham and Mannila (2001) that a much lower number of random projections than the bound gives a comparable performance, we investigate selected numbers ranging from 10 to 1000. Note that increasing the number of random projections may result in longer computation time. We intend to select a smaller number of random projections to ensure computational efficiency while maintaining accuracy in change point location identification, as well as ensuring acceptable sizes and powers.

First, we compare the effect of different change point tests when combined with RP. Figure 1 presents the sizes and size-adjusted powers of the RP methods using different change point tests with $k = 200$ and Bonf. The corresponding raw empirical rejection rates are provided in Figure S.8 in the Supplementary Material S.1.2. The change point location is set at $\theta = 0.25$. From Figure 1, among the different trimming choices of the weighted CUSUM tests, the trimming choice of $\lfloor n^{0.5} \rfloor$ leads to slightly higher size-adjusted powers but over-rejects. The trimming choice of $\lfloor \log(n) \rfloor$ has better sizes and similar size-adjusted powers as $\lfloor n^{0.5} \rfloor$ in most cases. We compare the weighted CUSUM test with trimming choice of $\lfloor \log(n) \rfloor$ and other tests. In the case of non-constant shift ($m = 5$ and $m = 20$), both the weighted CUSUM and the standard CUSUM have manifestly higher size-adjusted powers in *Settings 1-2*, followed by the HS test. The HR test exhibits the least powers. The weighted CUSUM exhibits slightly better size-adjusted powers in *Setting 3*, closely followed by the standard CUSUM, with the standard CUSUM controlling the sizes better. In the case of constant shift ($m = 1$), all the tests display low size-adjusted powers, while the weighted CUSUM and

standard CUSUM still outperform. From Figure S.8, the weighted CUSUM has the best powers, followed by the standard CUSUM, with the standard CUSUM controlling the sizes better. The DE test exhibits the least powers in most cases. Overall, Figure 1 and Figure S.8 suggest that the weighted CUSUM and the standard CUSUM test outperform the other change point tests in terms of size control and power. When the change point location is in the middle ($\theta = 0.5$) as presented in Figure S.6 and Figure S.7 in Supplementary Material S.1.2, the standard CUSUM test exhibits even superior performance, acquiring higher raw powers and size-adjusted powers in all the alternative cases than the weighted CUSUM test and other tests. While more extreme change point locations may change the results, as suggested in Horváth et al. (2020), it appears that as long as the change points are well within the observation boundaries, the standard CUSUM is a reasonable choice to combine with random projections. More results of the sizes and size-adjusted powers of the RP methods with BH, HMP, and CCT are presented in Figure S.12, Figure S.13 and Figure S.14, and the corresponding sizes and raw powers in Figure S.9, Figure S.10, and Figure S.11 in Supplementary Material S.1.2.

Secondly, we compare the effect of different p -value combination methods. Figure 2 presents the sizes and size-adjusted powers of the RP methods using different p -value combination methods with $k = 200$ and the standard CUSUM test. The corresponding raw empirical rejection rates are provided in Figure S.15 in Supplementary Material S.1.2. Denote RP-Bonf, RP-BH, RP-HMP, and RP-CCT by RP methods with p -value combination methods Bonf, BH, HMP and CCT, respectively. The change point location is set at $\theta = 0.25$. From Figure 2, when $m = 5$ and $m = 20$, the RP-Bonf method has the best size-adjusted powers in *Settings 1-2*, the RP-BH has the best size-adjusted powers in *Setting 3*. When $m = 1$, the four methods have similar size-adjusted powers, with the RP-HMP being slightly better in *Setting 1* and the RP-BH being slightly better in *Settings 2-3*. From Figure S.15, when $m = 5$ and $m = 20$, the RP-HMP method has slightly better raw powers. The other three methods lead to similar performance in terms of raw powers. When $m = 1$, the RP-HMP still performs best in raw powers, followed by the RP-CCT method, while the RP-Bonf method displays manifestly lower raw powers. Table 1 presents the empirical rejection rates under the null for the RP methods using different p -value combination methods with $k = 200$ and the CUSUM test, providing precise numerical comparisons. These results are visually presented in Figure 2 as well. More results of using different tests are provided in the Table S.1 in Supplementary Material S.1.2. From Tables 1 and S.1, both the RP-HMP and RP-CCT methods may lose size control. It is because these methods are valid only when the significance level is small enough, especially when dependence is weak. Conditioning on the data in the original dimension X , each projected univariate time series using RP are independent. For HMP and CCT, significance level of 0.05 may still be too large under independence, as Rho (2024) points out. In fact, considering the independence among RPs given the high dimensional data, Bonf and BH would

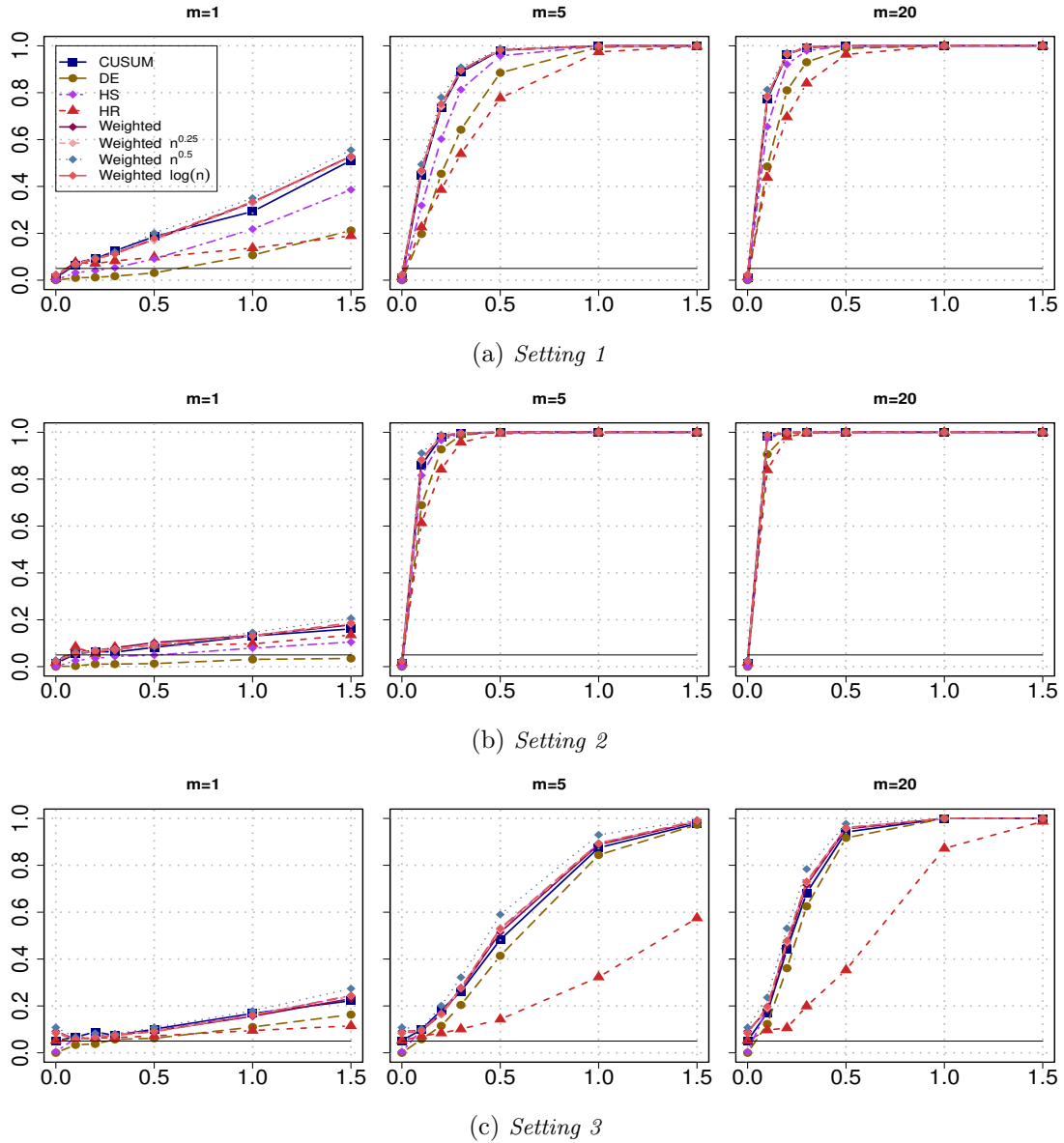


Figure 1: Adjusted empirical rejection rates of the RP methods for various values of SNR in the x-axis. The RP method performs 200 random projections and applies different change point tests (CUSUM, Weighted, DE, HS, HR) and the Bonf combination method. The data-generating process follows (3.2) where the standard deviation σ_g follows Settings 1-3. The change point location is set at $\theta = 0.25$. The empirical rejection rate is based on 1000 simulations.

work reasonably well. The RP-BH maintains appropriate rejection rates under the null in Settings 1-2 and the RP-Bonf shows the best performance in controlling the sizes in Setting 3. Overall, the RP-Bonf and RP-BH methods have better size-adjusted powers in most cases and control the sizes well. Considering that Bonf and BH can also naturally identify significant individual tests, unlike the sum-based methods such as HMP and CCT, we recommend using Bonf or BH with RP.

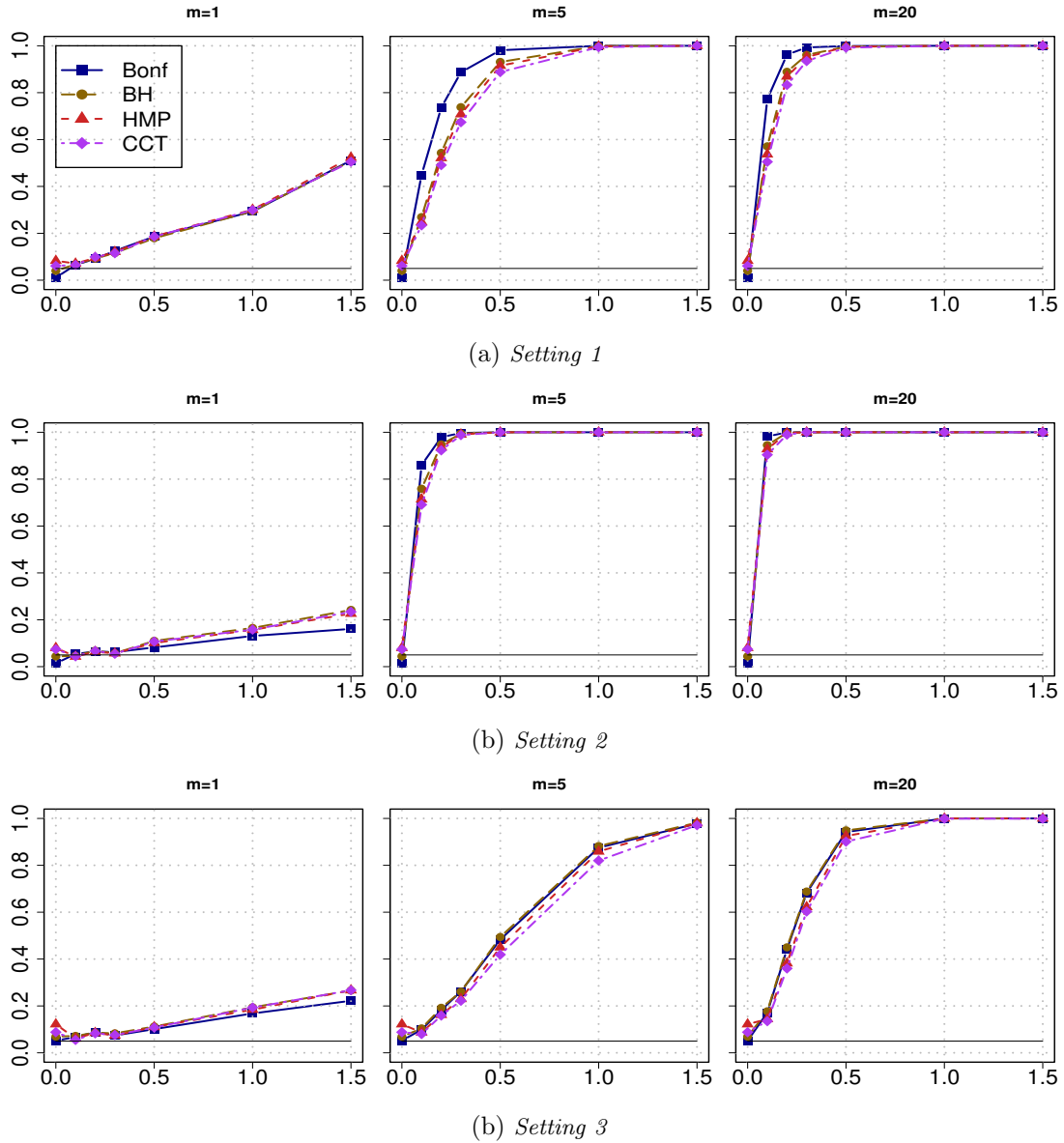


Figure 2: Adjusted empirical rejection rates of the RP-Bonf, RP-BH, RP-HMP, and RP-CCT methods with the standard CUSUM test for various values of SNR in the x-axis. The RP method performs 200 random projections. The data-generating process follows (3.2) where the standard deviation σ_g follows *Settings 1-3*. The change point location is set at $\theta = 0.25$. The empirical rejection rate is based on 1000 simulations.

Empirical rejection rate under the null (significance level 0.05)				
	Bonf	HMP	BH	CCT
<i>Setting 1</i>	0.011	0.083	0.040	0.061
<i>Setting 2</i>	0.014	0.080	0.044	0.074
<i>Setting 3</i>	0.052	0.122	0.069	0.088

Table 1: Empirical rejection rate under the null of RP method using different p -value combination methods with $k = 200$ and the standard CUSUM test.

Thirdly, we compare the effect of the RP methods with different numbers of random projections. Following the selected choices from Figures 1, we limit the change point test to standard CUSUM. We compare the sizes, raw powers, size-adjusted powers of our methods as well as root mean squared errors (RMSE) of estimated change point locations. The choices of the number k of random projections range from 10 to 100 in increments of 10 and then from 100 to 1000 in increments of 50.

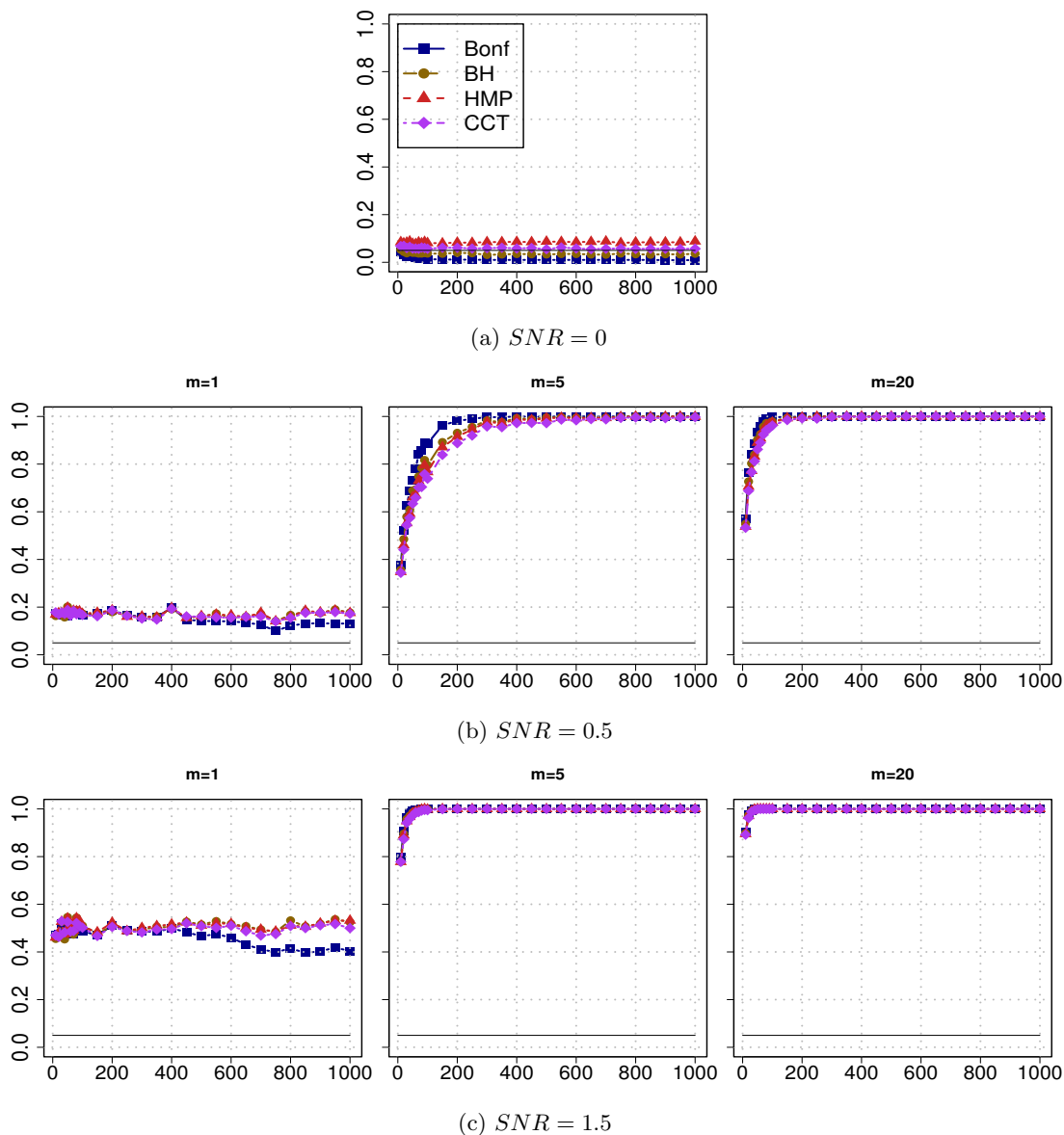


Figure 3: Adjusted empirical rejection rates of the RP-Bonf, RP-BH, RP-HMP and RP-CCT methods with the standard CUSUM test for various choices of number k of random projections in the x-axis. The data-generating process follows (3.2) where the standard deviation σ_g follows *Setting 1*. The change point location is set at $\theta = 0.25$. The empirical rejection rate is based on 1000 simulations.

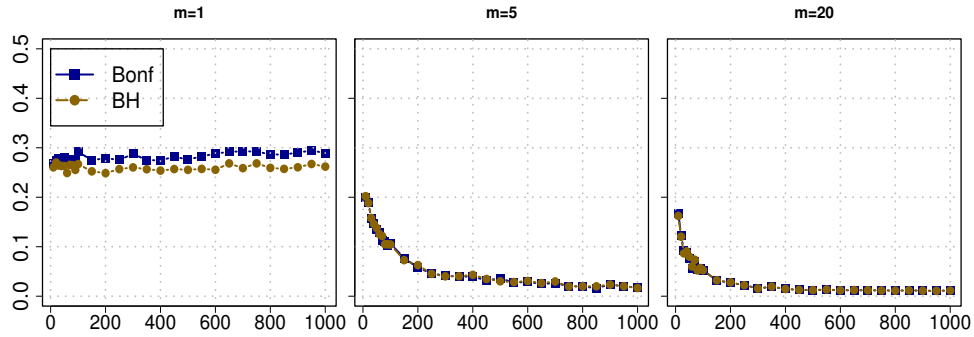
Figure 3 displays the sizes and size-adjusted powers of the RP methods in *Setting 1*. The results in

Settings 2 and *3* are provided in Figures [S.19](#) and [S.20](#) in Supplementary Material [S.1.2](#). The raw empirical rejection rates in *Settings 1-3* are presented in Figures [S.16](#), [S.17](#), and [S.18](#). The change point location is set at $\theta = 0.25$. In Figure [3](#), under the null ($SNR = 0$), the RP-BH method can control the sizes well across different numbers of random projections. The RP-HMP method tends to over-reject, similarly to what we observed in Table [1](#). Under the alternatives with $SNR = 0.5$ and $SNR = 1.5$, when $m = 5$ and $m = 20$, size-adjusted powers of the RP methods are improved significantly as the number k of random projections rises. Moreover, the size-adjusted powers remain stable after $k = 200$. However, when $m = 1$, the size-adjusted powers fluctuates without an ascending trend as k increases. Similar trends can be found in the raw powers.

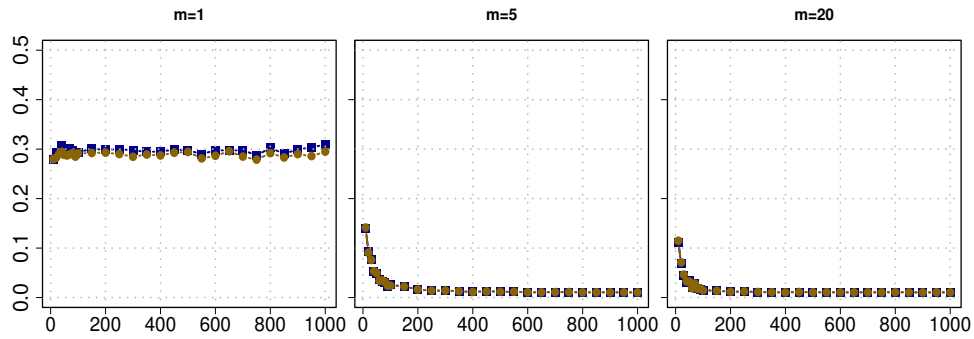
Figure [4](#) displays RMSE of all the estimated change point locations detected by the RP methods with an increasing number of random projections. We include non-significant ones because those are used later in Subsection [3.3](#) when repeating the RP methods and are appeared to be informative as well. We report the RMSE of only significant estimated change point locations in Figure [S.21](#) in Supplementary Material [S.1.2](#). The change point location is set at $\theta = 0.25$. In Figure [4](#), when $m = 5$ and 20 , RMSE exhibits a declining trend, decreasing rapidly at the beginning as the number k of random projections increases. It seems that $k = 200$ is enough in most cases. Beyond $k = 200$, further increases in the number of random projections does not result in a remarkable gain in RMSE. However, when $m = 1$, the RMSE is higher than that in $m = 5$ and 20 , and does not decline as k increases. The difficulty observed when $m = 1$ also arises in other comparable methods, as shown in Figure [5](#) in Subsection [3.2](#). This may be because, when $m = 1$, the break function is constant and the change is uniform across components with a small magnitude. In contrast, when $m = 5$ or $m = 20$, the break function is non-constant, and the change is different across components. Some components exhibit larger changes, which appear to be easier to detect. Therefore, for the data settings we consider, performing $k = 200$ random projections appears to be a reasonable choice for the RP methods, as it offers a simpler computation while maintaining similar performance as with much larger k . The additional random projections beyond $k = 200$ undermine the computational efficiency of the RP method. Figure [S.21](#) exhibits a trend similar to that in Figure [4](#), suggesting $k = 200$ but with lower RMSE values.

3.2 Comparison of change point methods

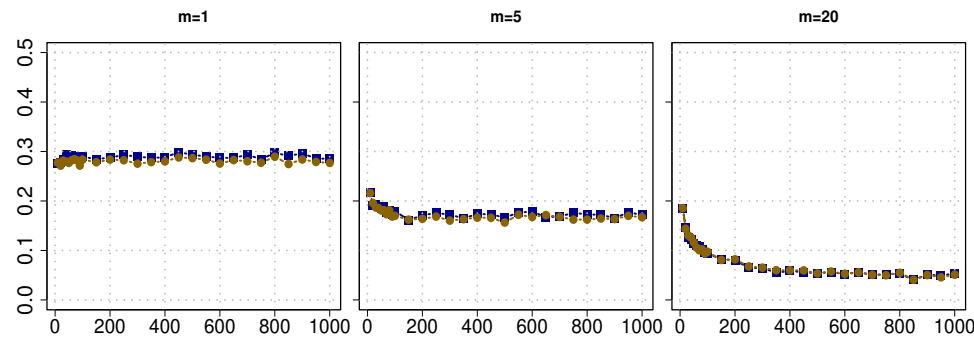
In this subsection, we compare the performance of the RP methods and other existing single change point detection methods for functional or high-dimensional data, including projection-based methods and functional methods without dimension reduction. Projection-based methods include FPC-based methods from [Aue et al. \(2009\)](#) and [Berkes et al. \(2009\)](#) with different desired proportion of total variation explained



(a) *Setting 1*



(b) *Setting 2*



(c) *Setting 3*

Figure 4: RMSE of estimated change point locations detected by the RP-Bonf and RP-BH methods with the standard CUSUM test for various choices of number k of random projections in the x -axis. The data-generating process follows (3.2) where the standard deviation σ_g follows *Settings 1-3*. The change point location is set at $\theta = 0.25$. The RMSE is based on 1000 simulations.

(TVE): 0.85, 0.90, and 0.95 (FPC-0.85, FPC-0.90, FPC-0.95), and a method from Wang and Samworth (2018), where one optimal direction that closely aligns with the direction of the change is identified. Methods without dimension reduction include a fully functional (FF) method from Aue et al. (2018) and a method from Dette et al. (2020).

In the process of change point detection, the RP methods, the FPC-based methods, and the FF method use a standard CUSUM process, while the methods in Wang and Samworth (2018) and Dette et al. (2020)

and use a weighted CUSUM process. We modify the methods in Wang and Samworth (2018) and Dette et al. (2020) to use the standard CUSUM process and label them as WS and DKV, respectively. The original versions of the two methods that use weighted CUSUM are labeled as WS-weighted and DKV-weighted. We present only the results of WS and DKV using the standard CUSUM process due to better size control in most cases in the considered settings than WS-weighted and DKV-weighted. The results of using weighted CUSUM are presented in the Figure S.22 in Subsection S.2 in the Supplementary Material. For Wang and Samworth (2018), we also consider their simulation-based approach to find a critical value. In our results, both WS and WS-CUSUM indicate Wang and Samworth (2018)'s method with standard CUSUM but with two different ways to compute critical values: WS chooses the 95% quantile of maximized standard CUSUM statistics of 1000 i.i.d. samples with no change point nor any temporal dependence, while the WS-CUSUM method rely on the simulation of Brownian bridges, similarly to the one described in the beginning of Subsection 3.1 for the weighted CUSUM.

We compare the aforementioned methods in terms of sizes, raw powers, and the accuracy of estimated change point locations. Figure 5 displays the empirical rejection rates of the RP method using 200 random projections and the other change point detection methods for high-dimensional or functional data. The change point location is set at $\theta = 0.25$. Under the null, our RP-BH method maintains an acceptable empirical rejection rate close to a significance level of 0.05 in *Settings 1-2*, while RP-Bonf method is conservative and RP-HMP is slightly over-rejecting. In *Setting 3*, our RP-Bonf shows the best performance in controlling the sizes compared to RP-BH and RP-HMP. For other methods, the WS method also controls the sizes well, comparable to our RP-BH in *Settings 1-2* and our RP-Bonf in *Setting 3*, followed by the FF method, while other methods fail to control the sizes.

Under the alternatives, when $m = 5$ and 20, our RP methods have the best power in *Settings 1-2*, followed by the WS-CUSUM method. In *Setting 2*, the projection-based methods show higher powers than methods without dimension reduction, though FPC with TVE 0.85 has lower power in weak and moderate alternative cases. Our RP methods show better performance compared to other projection-based methods. In *Setting 3*, FPC with TVE 0.95 and WS-CUSUM have higher power than our RP methods when magnitude of change is small ($SNR \leq 0.5$) but are outperformed by RP-HMP method when $SNR > 1$. When $m = 1$, RP-BH and RP-Bonf methods are surpassed by other projection-based methods, while RP-HMP exceeds WS method in all *Settings* and has comparable performance to FPC 0.85 method in *Setting 3*. Overall, our RP methods are recommended for detecting data with potentially non-constant break functions. Based on the comparison across the three *Settings*, RP-Bonf and RP-BH method is suggested when the variability of data is concentrated in few directions. When the data has variability across more directions, RP-HMP is applicable to detect change with relatively large magnitude.

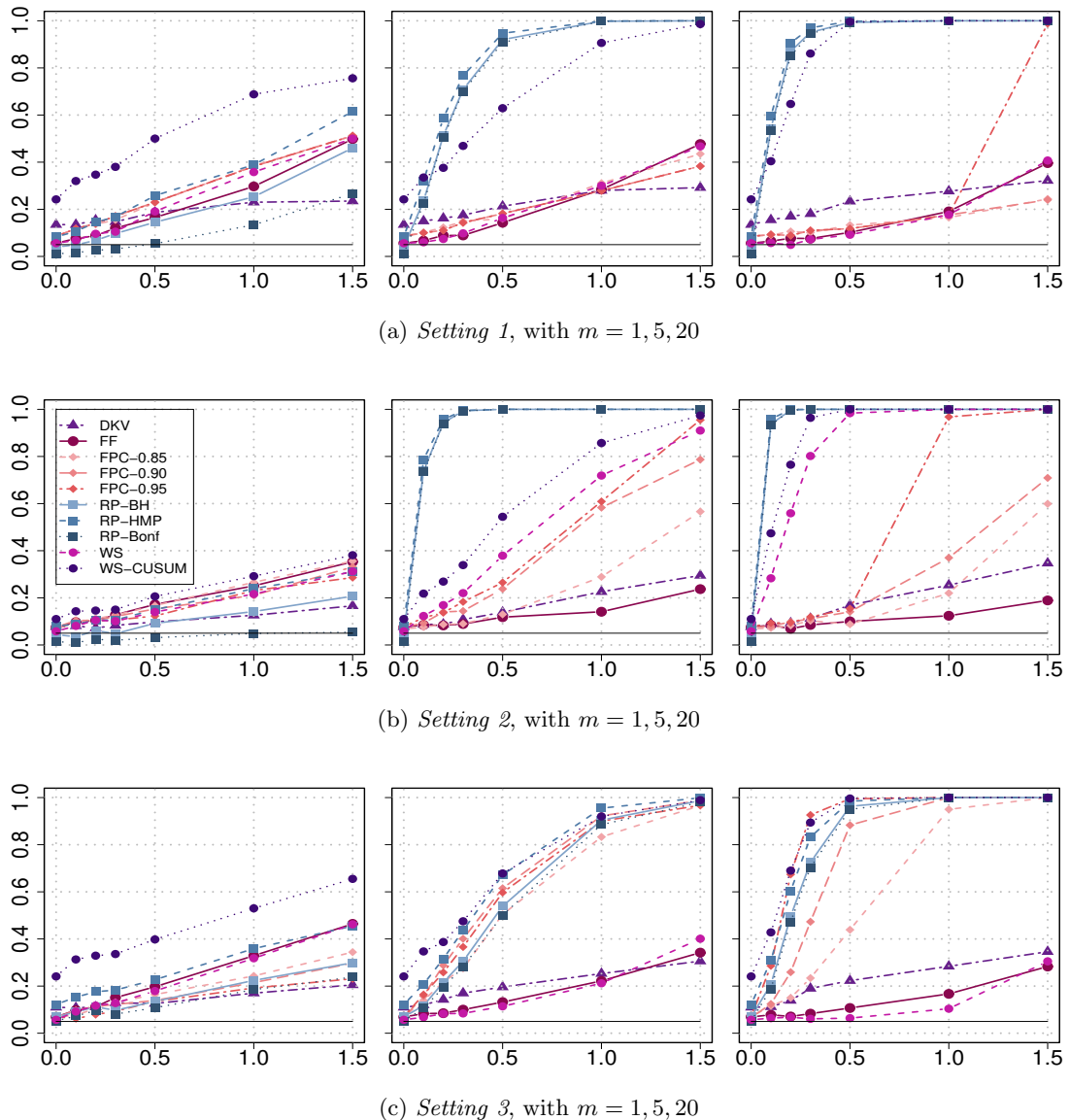
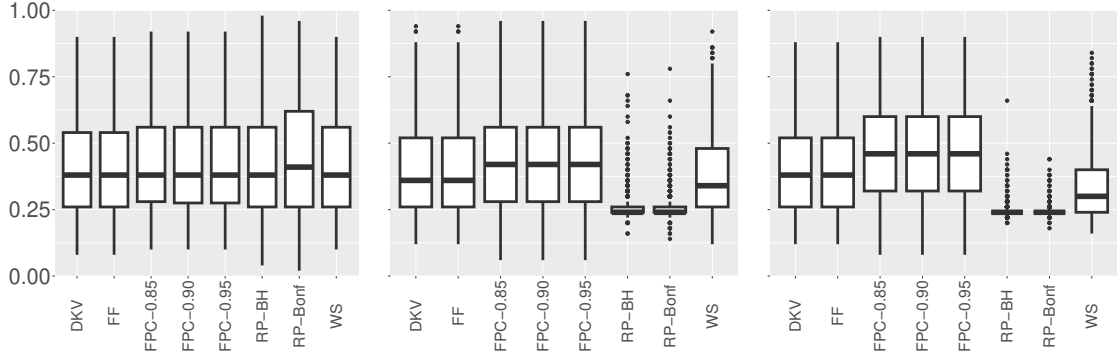
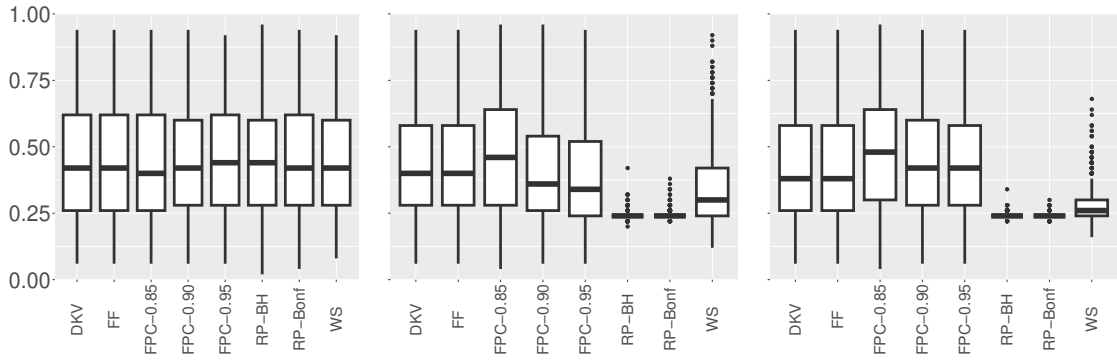


Figure 5: Raw empirical rejection rates of various change point detection methods, including projection-based and fully functional methods, for various values of SNR in the x -axis. The data-generating process follows (3.2) where the standard deviation σ_g follows *Settings 1-3*. The change point location is set at $\theta = 0.25$. The rejection rate is based on 1000 simulations.

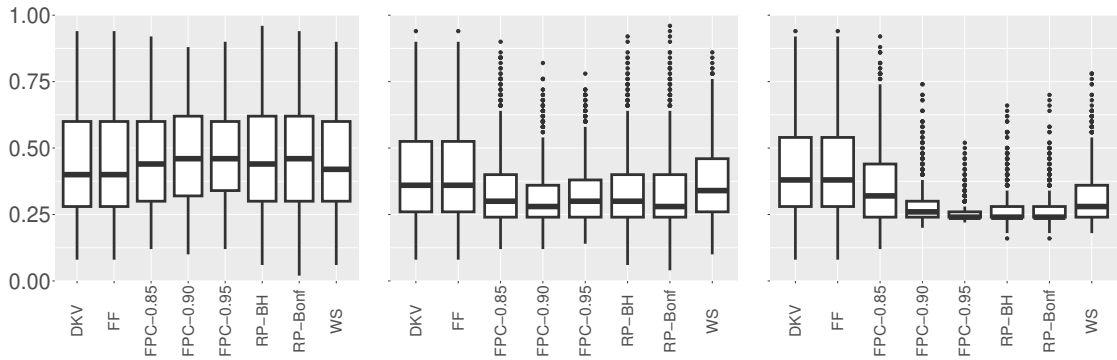
Figure 6 presents the boxplots of estimated change points detected by the aforementioned methods. Our RP methods use $k = 200$ random projections. The change point location is set at $\theta = 0.25$. The magnitude of the break function is scaled by $SNR = 0.5$. When $m = 5$ and 20 , in *Settings 1-2*, the RP methods can detect the change point most accurately, as the median is closely aligned with the true location 0.25 , followed by the WS method which has a wider spread. In *Setting 3*, the spread of our estimates is similar to that of FPC 0.9 with the median of our estimates being closer to the true location. The spread of our estimates



(a) *Setting 1*, with $m = 1, 5, 20$



(b) *Setting 2*, with $m = 1, 5, 20$



(c) *Setting 3*, with $m = 1, 5, 20$

Figure 6: Estimated change point locations detected by different methods on 1000 simulations. The data-generating process follows (3.2) where the standard deviation σ_g follows *Settings 1-3*. The change point location is set at $\theta = 0.25$. The magnitude of the break function is scaled by $SNR = 0.5$.

is narrower than other methods when $m = 20$, except for FPC 0.95. When $m = 1$, the RP methods do not have distinct advantages. The RP methods are similar to the WS method in both median and spread. However, when $m = 1$, methods without dimension reduction (DKV, FF) show advantages in *Setting 3*, as their medians are closer to the true location. Overall, given the high accuracy and precision, RP methods

are well-suited for applications with non-constant break function. In the case of constant break function, methods without dimension reduction may be preferable.

3.3 Location estimates of the RP method in practice

The location estimates based on RP methods may be unstable due to the randomness of directions. In practice, we propose to repeat RP-BH (or RP-Bonf) method multiple times to achieve stability. We compare the quality of location estimates of RP-based methods with those of existing methods in simulations: fix a single simulated dataset, and repeat each RP-BH (or RP-Bonf) method 1000 times. We consider $k = 200$ random projections and the standard CUSUM. The change point location is set at $\theta = 0.25$. The magnitude of the break function is scaled by $SNR = 0.5$. Figure 7 summarizes the resulting empirical distributions of the 1000 estimated change point locations using violin plots, with the red dot indicating the mode across all 1000 repetitions for RP-BH and RP-Bonf. We also report the estimated change point locations only when a 200-RP set leads to a significant adjusted p -values: $\min_{1 \leq r \leq 200} p_{adj}(r) < 0.05$. These methods are labeled as RP_BH_sig and RP_Bonf_sig. Figure S.23 in Supplementary Material S.3 includes those results. While RP_BH_sig and RP_Bonf_sig may have smaller variability compared to those using all 1000 change location estimates, they may miss detecting some changes, especially when $m = 1$.

Four additional figures similar to Figure 7 are presented as Figures S.24-S.27 in Section S.3 in the Supplementary Material. These figures are the same as Figure 7, except that they are based on different datasets. In most cases, the RP methods exhibit less variability when $m = 5$ and $m = 20$ than $m = 1$, especially in *Settings 1-2*. When $m = 5$ and $m = 20$, though repeating the RP method can yield variable estimated locations, the mode of the RP repetitions is accurate in most cases, tending to be closer to the true location than other methods. When $m = 1$, the mode of the RP repetitions is similar to the locations obtained by other methods in most datasets.

In practice, we recommend repeating the RP method. If the detected change points across repeated RP methods are consistent, a small number of repetition would be okay. However, if they vary widely, we recommend repeating the RP method many times, for example, 1000 times, and choosing an aggregate estimate, for example, the mode. The mode across repetitions can be reported as the final change point estimate because it targets the most frequently reproducible change point location, and is less influenced by outlier estimates. When the distribution has multi peaks, it might be an indication that there exist multiple change points, or the mean change is more gradual rather than abrupt. This related topic of detecting multiple change points will be discussed further in separate work.

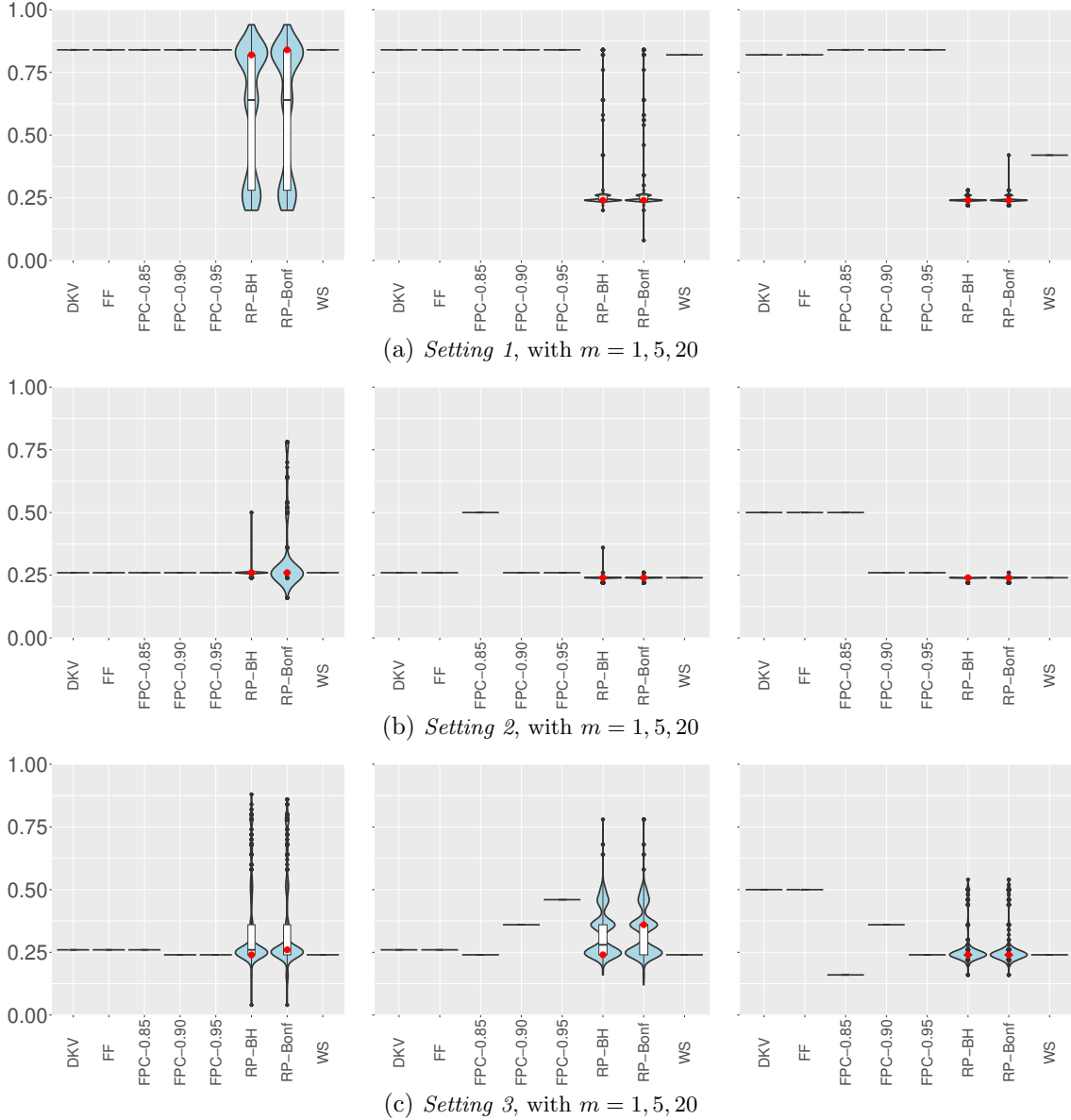


Figure 7: Estimated change point locations detected by repeating the methods on one dataset (Dataset 1) 1000 times. For the RP methods, the mode of the estimated locations across the 1000 repetitions is marked by a red dot. The data-generating process follows (3.2) where the standard deviation σ_g follows Settings 1-3. The change point location is set at $\theta = 0.25$. The magnitude of the break function is scaled by $SNR = 0.5$.

4 Application

We illustrate the performance of the RP method using daily minimum temperatures from eight Australian weather stations, most of which provide records spanning more than 100 years. The station names and numbers are Boulia (038003), Cape Otway (090015), Gayndah (039066), Gunnedah (055024), Hobart (094029), Melbourne (086338), Robe (026026), and Sydney (066214). The dataset is available from the Australian Bureau of Meteorology's on the following website <http://www.bom.gov.au/climate/data/acorn-sat/>, which

provide long-term climate monitoring. Our objective is to identify the year that the mean shift starts. For each station, we form a yearly sequence $\{\mathbf{x}_t\}_{t=1}^n$, where $n = 114$ for most stations. We remove the extra day in leap years, resulting in $p = 365$ observations per year. We apply the RP-Bonf method with $k = 200$ random projections and the standard CUSUM test. Because the estimated change point location can vary across different runs, we repeat the RP-Bonf method 1000 times on each station’s dataset and report the mode, following the procedure in Subsection 3.3. Figure 8 presents the empirical distribution of detected change point locations across the 1000 repetitions and highlights the mode, where six stations have common time range 1910 – 2023. The remaining two stations have different ranges, 1948 – 2023 and 1918 – 2023. From Figure 8, the stations Gayndah, Gunnedah, Hobart, Robe, and Sydney seem to form a sharp peak, indicating that the same calendar year is repeatedly selected across many RP repetitions. In these cases, the mode provides a stable and reproducible estimate of the change point location. The other stations Boulia, Cape Otway, and Melbourne have more than one peak, suggesting that multiple candidates years or gradual mean transition.

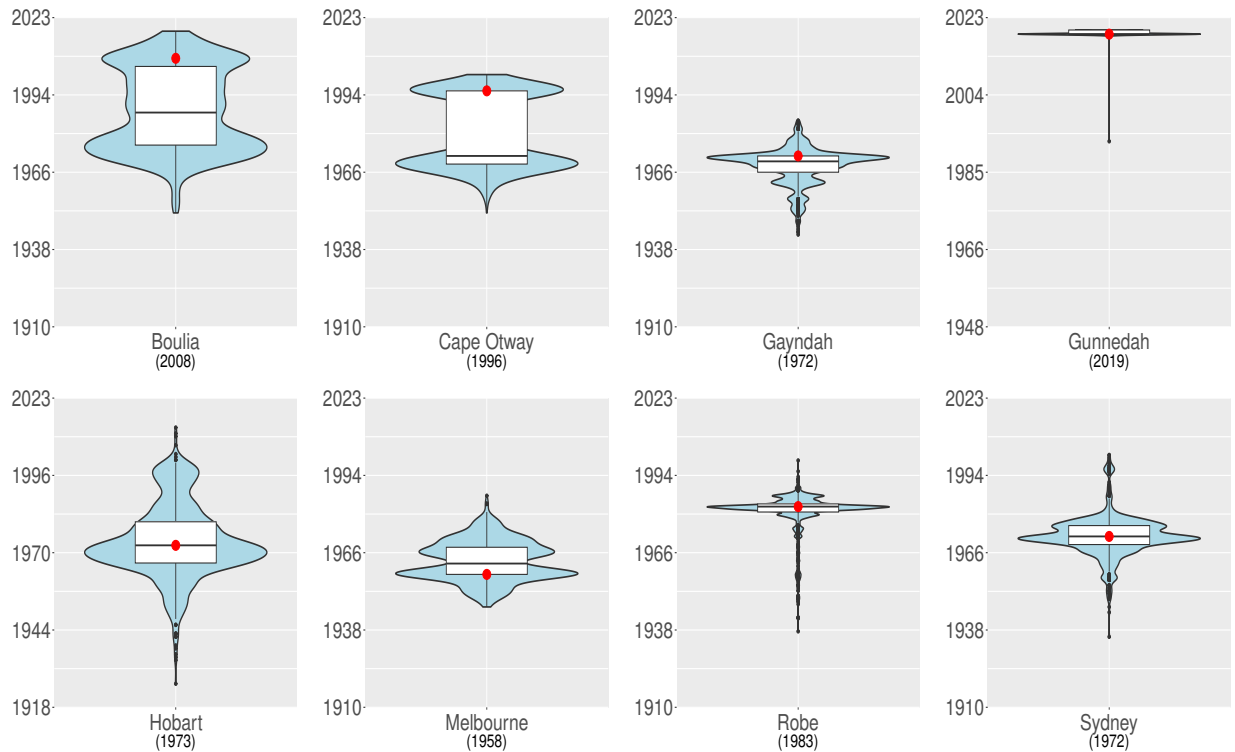


Figure 8: Estimated change point locations detected by repeating the RP-Bonf method on the temperature dataset 1000 times. The mode of the estimated locations across the 1000 repetitions is marked by a red dot and labeled in the parenthesis under the station.

5 Conclusion

This paper proposes a random projection change point detection method in high-dimensional data. By projecting high-dimensional data onto multiple random directions and applying a standard univariate change point test on each projected series, the proposed method converts a high-dimensional problem into a collection of one-dimensional tasks, which is computationally easy and offers more methods to use. The family-wise error or false discovery rate is controlled by aggregating across projections using a p -value combination method. Our simulation results show that the RP method has better size control, higher power, and accurate location detection when the break function is not constant in the considered cases. At the same time, the change location estimate of the RP methods may have high variability. We handle it by repeating RP methods and reporting the mode over repetitions. The real-data analysis illustrates how the proposed RP method can be used in practice. In summary, the RP method provides a computationally easy and conceptually simple approach for change point analysis in high dimensions.

The scope of this paper is limited to the single change point case. Extending the scope to cover multiple change points would strengthen applicability. This topic will be discussed in a future work using binary segmentation as a breakthrough.

Acknowledgement

Rho was partially supported by NIH-R15GM135806.

References

- Achlioptas, D. (2003). Database-friendly random projections: Johnson-lindenstrauss with binary coins. *Journal of computer and System Sciences* 66(4), 671–687.
- Aminikhanghahi, S. and D. J. Cook (2017). A survey of methods for time series change point detection. *Knowledge and information systems* 51(2), 339–367.
- Andrews, D. W. (1991). Heteroskedasticity and autocorrelation consistent covariance matrix estimation. *Econometrica: Journal of the Econometric Society*, 817–858.
- Andrews, D. W. (1993). Tests for parameter instability and structural change with unknown change point. *Econometrica: Journal of the Econometric Society*, 821–856.
- Arriaga, R. I. and S. Vempala (1999). An algorithmic theory of learning: Robust concepts and random

- projection. In *40th Annual Symposium on Foundations of Computer Science (Cat. No. 99CB37039)*, pp. 616–616. IEEE Computer Society.
- Aston, J. A. and C. Kirch (2012a). Detecting and estimating changes in dependent functional data. *Journal of Multivariate Analysis* 109, 204–220.
- Aston, J. A. and C. Kirch (2018). High dimensional efficiency with applications to change point tests. *Electronic Journal of Statistics* 12(1), 1901 – 1947.
- Aston, J. A. D. and C. Kirch (2012b). Evaluating stationarity via change-point alternatives with applications to fMRI data. *The Annals of Applied Statistics* 6(4), 1906 – 1948.
- Aue, A., R. Gabrys, L. Horváth, and P. Kokoszka (2009). Estimation of a change-point in the mean function of functional data. *Journal of Multivariate Analysis* 100(10), 2254–2269.
- Aue, A. and L. Horváth (2013). Structural breaks in time series. *Journal of Time Series Analysis* 34(1), 1–16.
- Aue, A., G. Rice, and O. Sönmez (2018). Detecting and dating structural breaks in functional data without dimension reduction. *Journal of the Royal Statistical Society. Series B (Statistical Methodology)* 80(3), 509–529.
- Bai, J. (2010). Common breaks in means and variances for panel data. *Journal of Econometrics* 157(1), 78–92.
- Benjamini, Y. and Y. Hochberg (1995). Controlling the false discovery rate: a practical and powerful approach to multiple testing. *Journal of the Royal statistical society: series B (Methodological)* 57(1), 289–300.
- Benjamini, Y. and D. Yekutieli (2001). The control of the false discovery rate in multiple testing under dependency. *The Annals of Statistics* 29(4), 1165 – 1188.
- Berkes, I., R. Gabrys, L. Horváth, and P. Kokoszka (2009). Detecting changes in the mean of functional observations. *Journal of the Royal Statistical Society: Series B (Statistical Methodology)* 71(5), 927–946.
- Bingham, E. and H. Mannila (2001). Random projection in dimensionality reduction: applications to image and text data. In *Proceedings of the seventh ACM SIGKDD international conference on Knowledge discovery and data mining*, pp. 245–250.
- Bonferroni, C. (1936). Teoria statistica delle classi e calcolo delle probabilita. *Pubblicazioni del R Istituto Superiore di Scienze Economiche e Commerciali di Firenze* 8, 3–62.

- Chan, J., L. Horváth, and M. Hušková (2013). Darling–erdős limit results for change-point detection in panel data. *Journal of Statistical Planning and Inference* 143(5), 955–970.
- Cho, H. (2016). Change-point detection in panel data via double CUSUM statistic. *Electronic Journal of Statistics* 10(2), 2000 – 2038.
- Csörgö, M. and L. Horváth (1993). *Weighted approximations in probability and statistics*. Wiley series in probability and statistics. Chichester, England; New York, NY: John Wiley & Sons.
- Csörgö, M. and L. Horváth (1997). *Limit theorems in change-point analysis*. Wiley series in probability and statistics. Chichester, England; New York, NY: John Wiley & Sons.
- Darling, D. A. and P. Erdős (1956). A limit theorem for the maximum of normalized sums of independent random variables. *Duke Mathematical Journal* 23(1), 143 – 155.
- Dasgupta, S. (2000). Experiments with random projection. In *Proceedings of the Sixteenth Conference on Uncertainty in Artificial Intelligence, UAI'00*, San Francisco, CA, USA, pp. 143–151. Morgan Kaufmann Publishers Inc.
- Dasgupta, S. and A. Gupta (2003). An elementary proof of a theorem of johnson and lindenstrauss. *Random Structures & Algorithms* 22(1), 60–65.
- Dette, H., K. Kokot, and S. Volgushev (2020). Testing relevant hypotheses in functional time series via self-normalization. *Journal of the Royal Statistical Society Series B* 82(3), 629–660.
- Enikeeva, F. and Z. Harchaoui (2019). High-dimensional change-point detection under sparse alternatives. *The Annals of Statistics* 47(4), 2051 – 2079.
- Ghojogh, B., A. Ghodsi, F. Karray, and M. Crowley (2021). Johnson-lindenstrauss lemma, linear and nonlinear random projections, random fourier features, and random kitchen sinks: Tutorial and survey. *arXiv preprint arXiv:2108.04172*.
- Hidalgo, J. and M. H. Seo (2013). Testing for structural stability in the whole sample. *Journal of Econometrics* 175(2), 84–93.
- Horváth, L. and M. Hušková (2012). Change-point detection in panel data. *Journal of Time Series Analysis* 33(4), 631–648.
- Horváth, L., P. Kokoszka, and G. Rice (2014). Testing stationarity of functional time series. *Journal of Econometrics* 179(1), 66–82.

- Horváth, L., C. Miller, and G. Rice (2020). A new class of change point test statistics of rényi type. *Journal of Business & Economic Statistics* 38(3), 570–579.
- Horváth, L. and G. Rice (2014). Extensions of some classical methods in change point analysis. *Test* 23(2), 219–255.
- Jiao, S., N.-H. Chan, and C.-Y. Yau (2022). Enhanced change-point detection in functional means. *arXiv preprint arXiv:2205.04299*.
- Jirak, M. (2015). Uniform change point tests in high dimension. *The Annals of Statistics*, 2451–2483.
- Johnson, W. B. and J. Lindenstrauss (1984). Extensions of lipschitz mappings into hilbert space. *Contemporary mathematics* 26, 189–206.
- Lee, J. R., M. Mendel, and A. Naor (2005). Metric structures in l_1 : dimension, snowflakes, and average distortion. *European Journal of Combinatorics* 26(8), 1180–1190.
- Li, P., T. J. Hastie, and K. W. Church (2006). Very sparse random projections. In *Proceedings of the 12th ACM SIGKDD international conference on Knowledge discovery and data mining*, pp. 287–296.
- Liu, B., X. Zhang, and Y. Liu (2022). High dimensional change point inference: Recent developments and extensions. *Journal of Multivariate Analysis* 188, 104833.
- Liu, B., C. Zhou, X. Zhang, and Y. Liu (2020). A unified data-adaptive framework for high dimensional change point detection. *Journal of the Royal Statistical Society Series B: Statistical Methodology* 82(4), 933–963.
- Liu, Y. and J. Xie (2020). Cauchy combination test: a powerful test with analytic p-value calculation under arbitrary dependency structures. *Journal of the American Statistical Association* 115(529), 393–402.
- Page, E. (1955). A test for a change in a parameter occurring at an unknown point. *Biometrika* 42(3/4), 523–527.
- Page, E. S. (1954). Continuous inspection schemes. *Biometrika* 41(1/2), 100–115.
- Rho, Y. (2024). Heavy-tailed p -value combinations from the perspective of extreme value theory. *arXiv preprint arXiv:2402.03197*.
- Wang, G. and L. Feng (2023). Computationally efficient and data-adaptive changepoint inference in high dimension. *Journal of the Royal Statistical Society Series B: Statistical Methodology* 85(3), 936–958.

- Wang, R., C. Zhu, S. Volgushev, and X. Shao (2022). Inference for change points in high-dimensional data via selfnormalization. *The Annals of Statistics* 50(2), 781–806.
- Wang, T. and R. J. Samworth (2018). High dimensional change point estimation via sparse projection. *Journal of the Royal Statistical Society. Series B (Statistical Methodology)* 80(1), 57–83.
- Wilson, D. J. (2019). The harmonic mean p-value for combining dependent tests. *Proceedings of the National Academy of Sciences* 116(4), 1195–1200.
- Yu, M. and X. Chen (2021). Finite sample change point inference and identification for high-dimensional mean vectors. *Journal of the Royal Statistical Society Series B: Statistical Methodology* 83(2), 247–270.

Supplementary Material on “Change point analysis of high-dimensional data using random projections”

YI XU AND YEONWOO RHO²

Department of Mathematical Sciences, Michigan Technological University

March 4, 2026

The supplementary material presents additional simulation results. Section [S.1](#) presents additional results for the parameter choice, relating to Section [3.1](#): Subsection [S.1.1](#) presents the results of the RP method using HAC estimator, and Subsection [S.1.2](#) presents the results of the RP method using [Horváth et al. \(2020\)](#)'s variance estimator $\hat{\sigma}_z^2 = \frac{1}{n}[(\sum_{t=1}^z (y_t - \bar{y}_z)^2 + \sum_{t=z+1}^n (y_t - \bar{y}_{n-z})^2)]$. Section [S.2](#) presents estimated change locations using weighted CUSUM approaches. Section [S.3](#) presents figures similar to Figure [7](#) in Section [3.3](#) but with different datasets.

²Author of Correspondence: Y. Rho (yrho@mtu.edu)

S.1 Additional results for Subsection 3.1

S.1.1 Results of using the HAC variance estimator

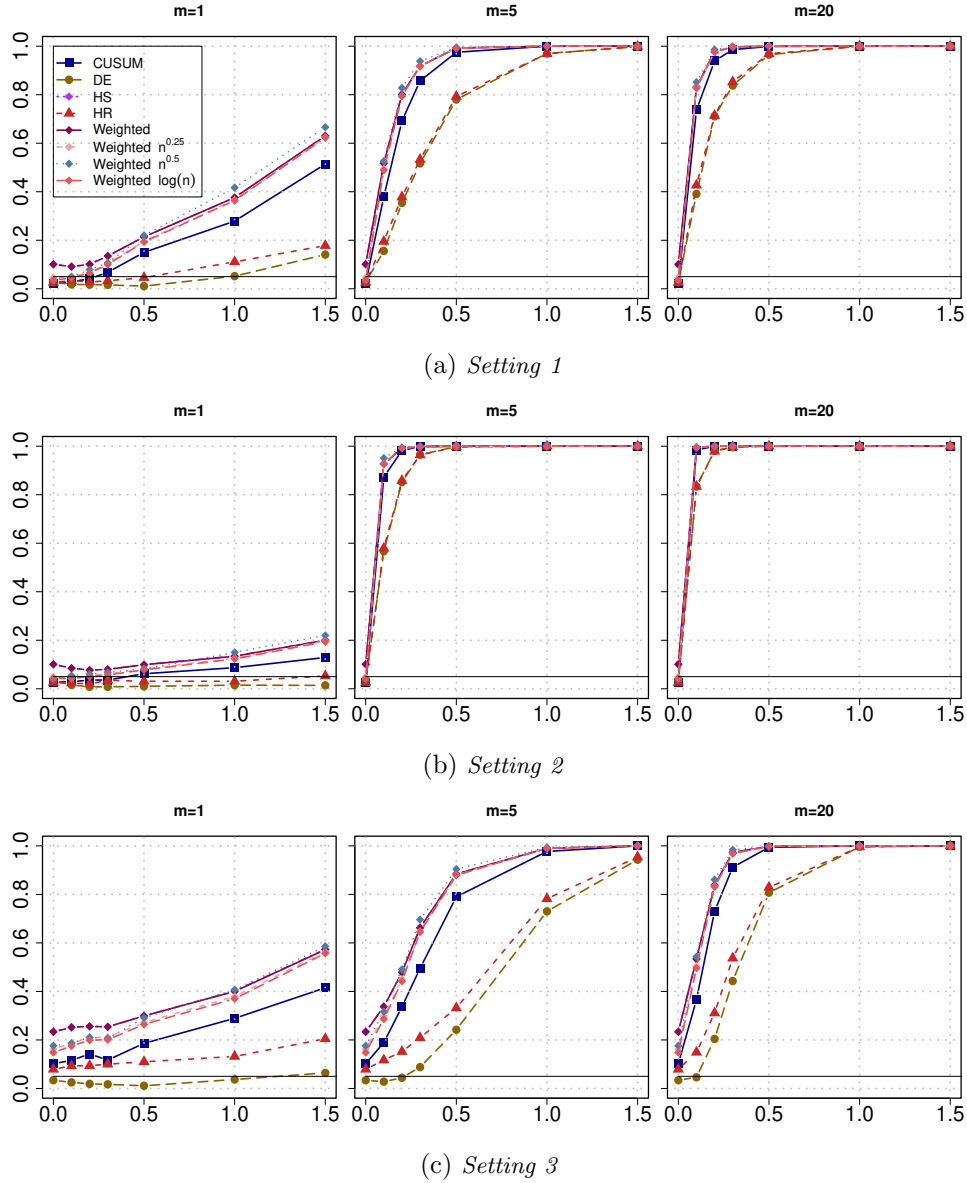
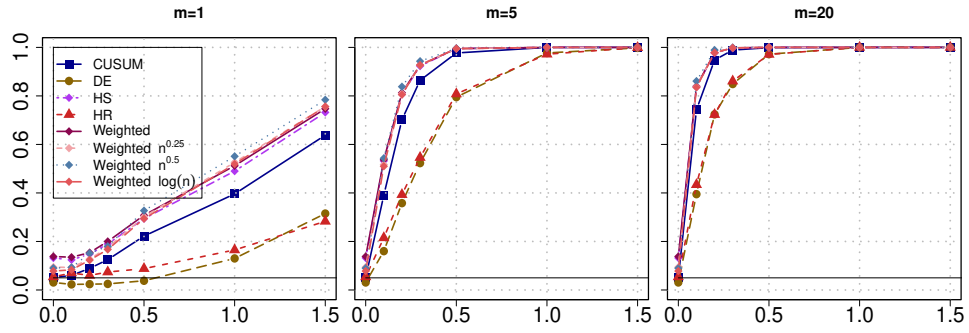
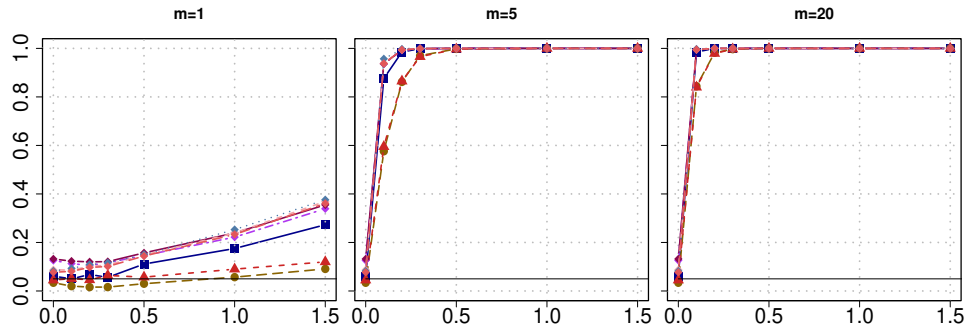


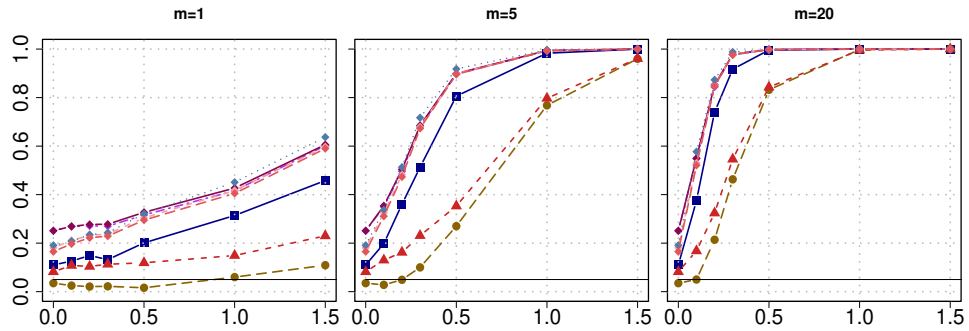
Figure S.1: Raw empirical rejection rates of the RP methods for various values of SNR in the x-axis. The RP method performs 200 random projections and applies different change point tests (CUSUM, Weighted, DE, HS, HR) and the Bonf combination method. The data-generating process follows (3.2) where the standard deviation σ_g follows *Settings 1-3*. The change point location is set at $\theta = 0.25$. The empirical rejection rate is based on 1000 simulations.



(a) *Setting 1*

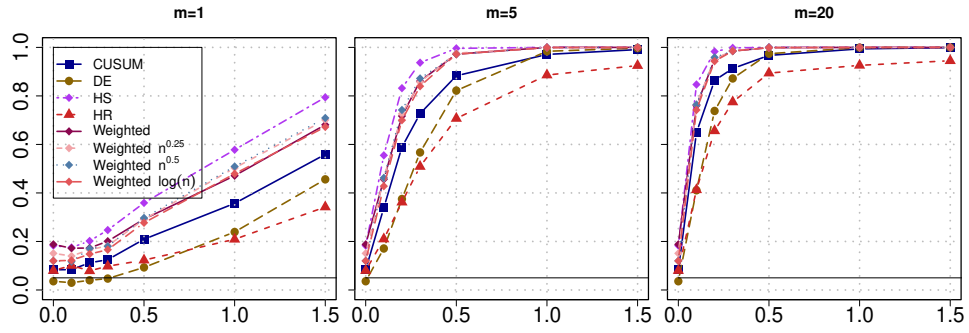


(b) *Setting 2*

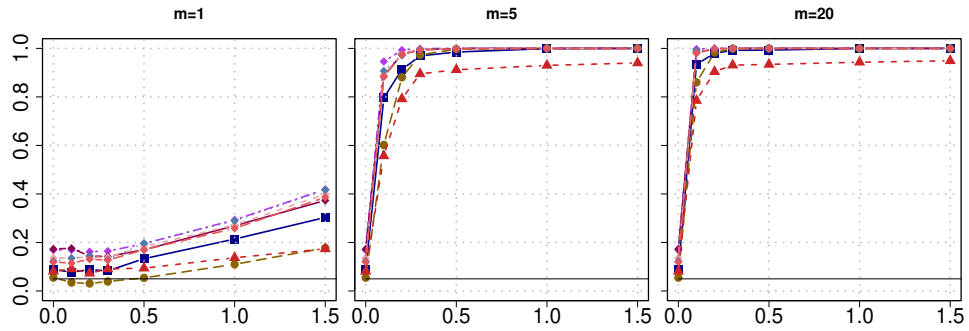


(c) *Setting 3*

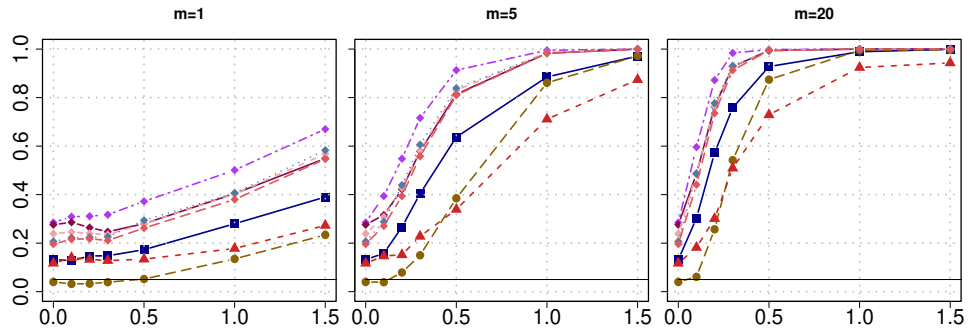
Figure S.2: Raw empirical rejection rates of the RP methods for various values of SNR in the x-axis. The RP method performs 200 random projections and applies different change point tests (CUSUM, Weighted, DE, HS, HR) and the BH combination method. The data-generating process follows (3.2) where the standard deviation σ_g follows *Settings 1-3*. The change point location is set at $\theta = 0.25$. The empirical rejection rate is based on 1000 simulations.



(a) Setting 1

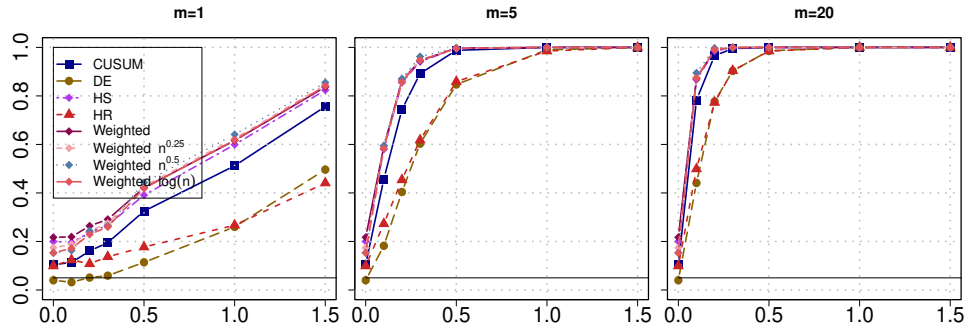


(b) Setting 2

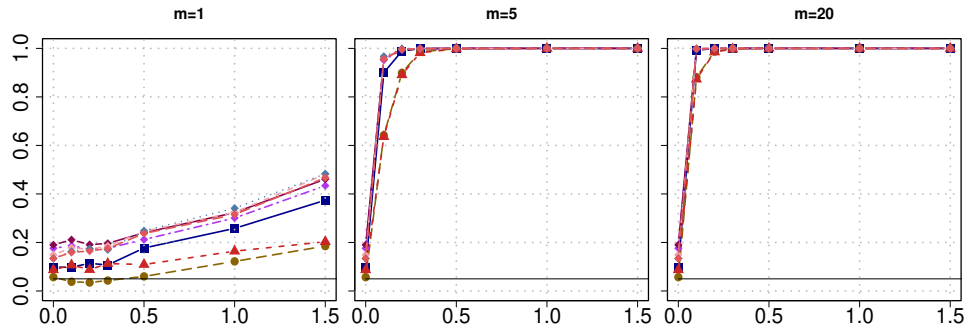


(c) Setting 3

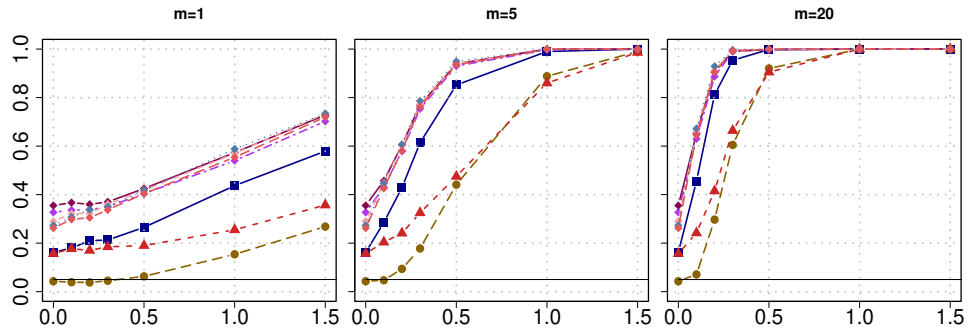
Figure S.3: Raw empirical rejection rates of the RP methods for various values of SNR in the x-axis. The RP method performs 200 random projections and applies different change point tests (CUSUM, Weighted, DE, HS, HR) and the CCT combination method. The data-generating process follows (3.2) where the standard deviation σ_g follows Settings 1-3. The change point location is set at $\theta = 0.25$. The empirical rejection rate is based on 1000 simulations.



(a) Setting 1

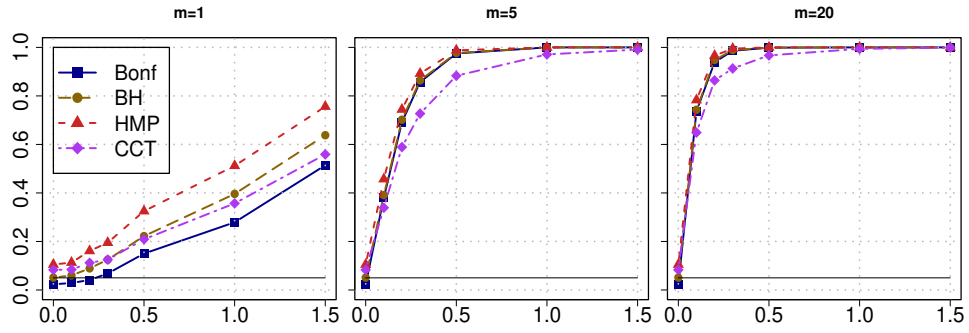


(b) Setting 2

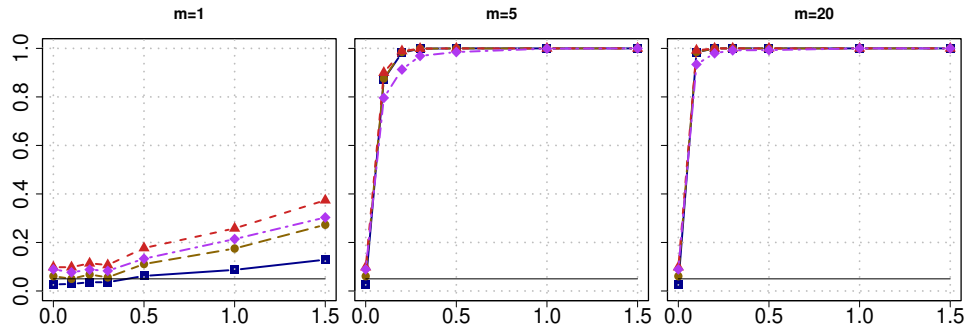


(c) Setting 3

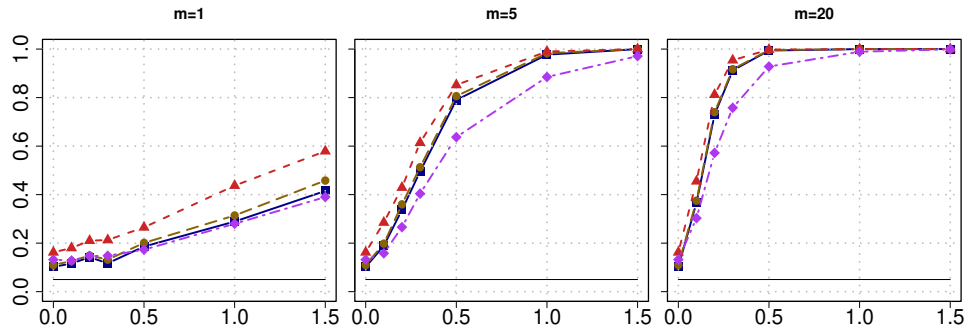
Figure S.4: Raw empirical rejection rates of the RP methods for various values of SNR in the x-axis. The RP method performs 200 random projections and applies different change point tests (CUSUM, Weighted, DE, HS, HR) and the HMP combination method. The data-generating process follows (3.2) where the standard deviation σ_g follows Settings 1-3. The change point location is set at $\theta = 0.25$. The empirical rejection rate is based on 1000 simulations.



(a) *Setting 1*



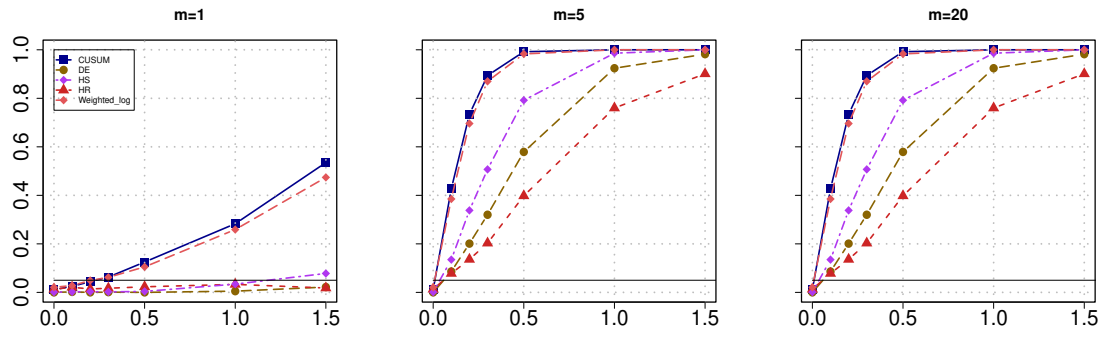
(b) *Setting 2*



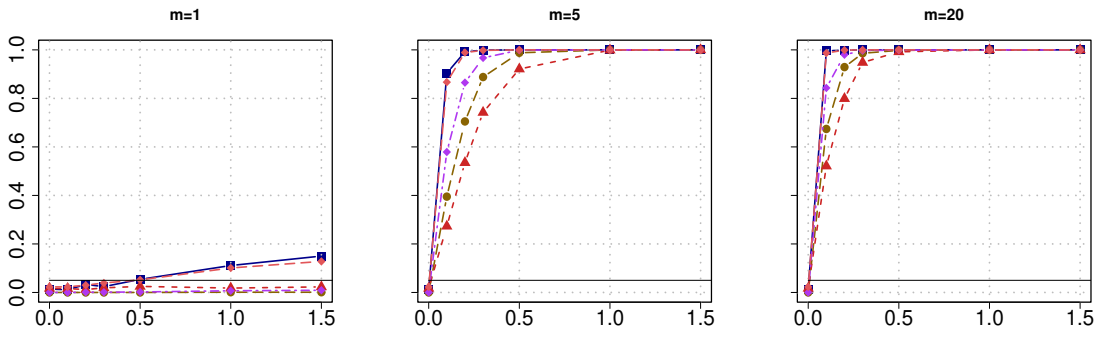
(c) *Setting 3*

Figure S.5: (HAC) Raw empirical rejection rates of the RP-Bonf, RP-BH, RP-HMP, and RP-CCT methods with the standard CUSUM test for various values of SNR in the x-axis. The RP method performs 200 random projections. The data-generating process follows (3.2) where the standard deviation σ_g follows *Settings 1-3*. The change point location is set at $\theta = 0.25$. The empirical rejection rate is based on 1000 simulations.

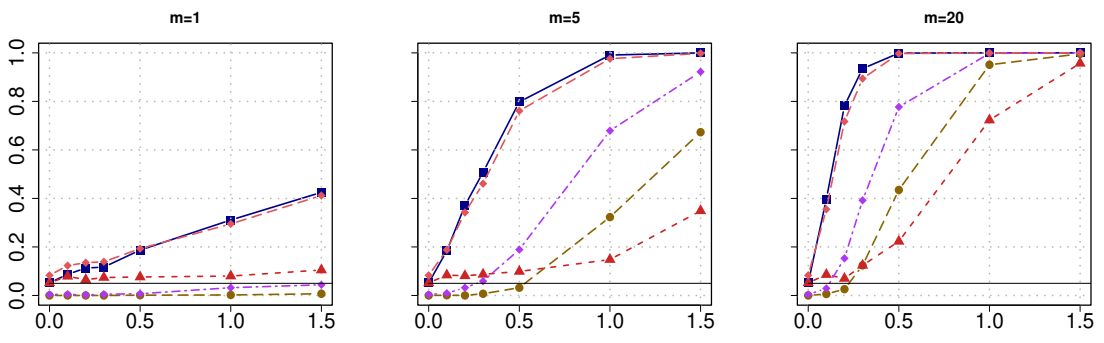
S.1.2 Results using the variance estimator in Horváth et al. (2020)



(a) Setting 1, with $m = 1, 5, 20$

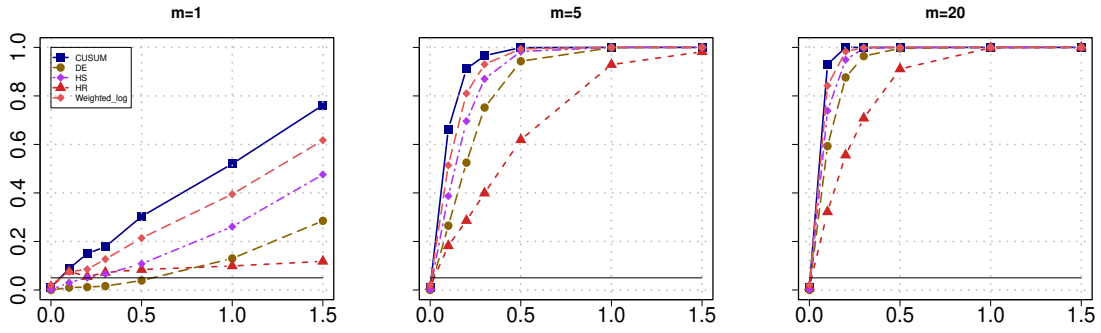


(b) Setting 2, with $m = 1, 5, 20$

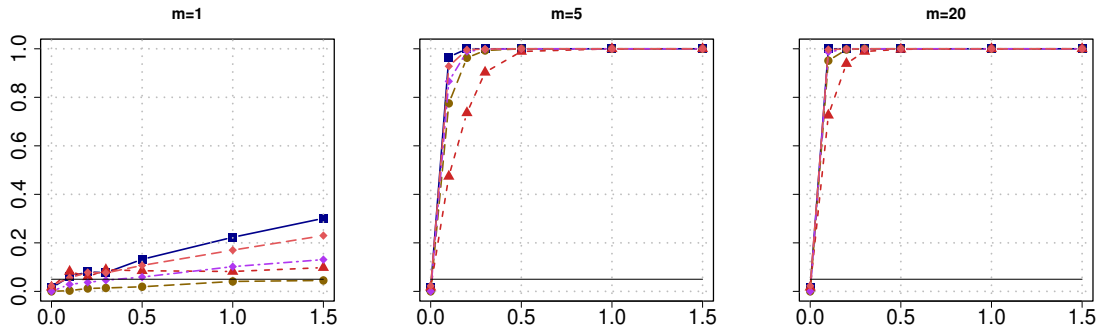


(c) Setting 3, with $m = 1, 5, 20$

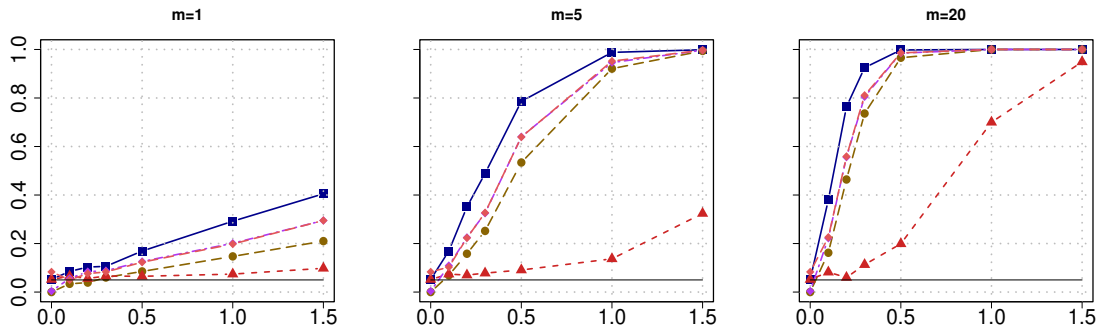
Figure S.6: Raw empirical rejection rates of RP-Bonf method using different change point tests with $k = 200$ in simulated data with $\theta = 0.5$.



(a) *Setting 1*, with $m = 1, 5, 20$

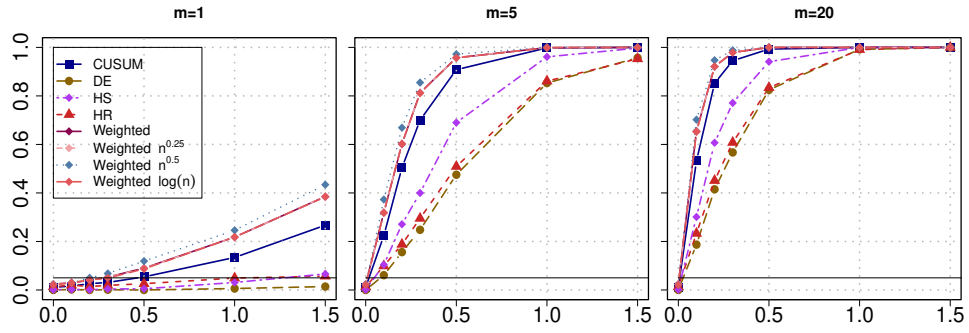


(b) *Setting 2*, with $m = 1, 5, 20$

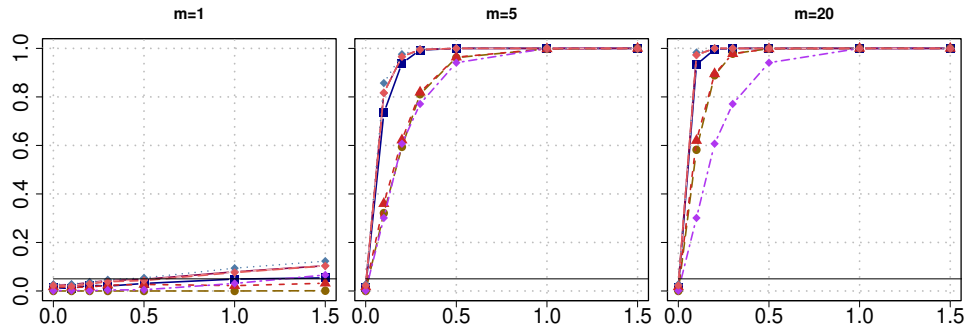


(c) *Setting 3*, with $m = 1, 5, 20$

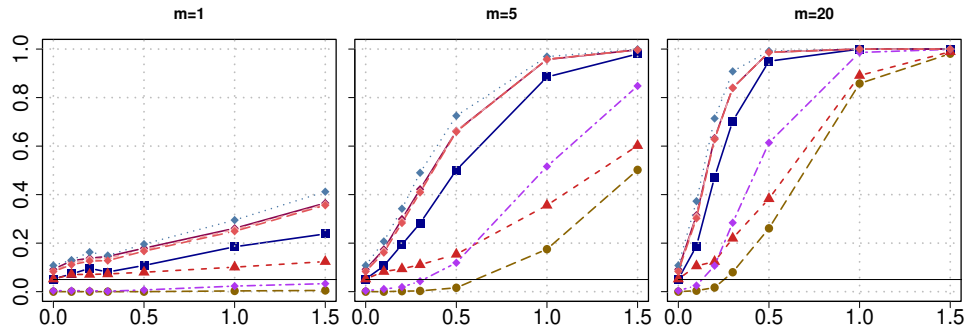
Figure S.7: Adjusted empirical rejection rates of RP-Bonf method using different change point tests with $k = 200$ in simulated data with $\theta = 0.5$.



(a) *Setting 1*

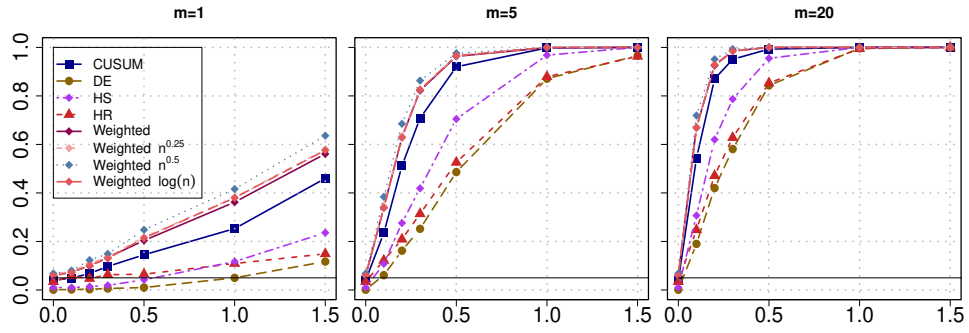


(b) *Setting 2*

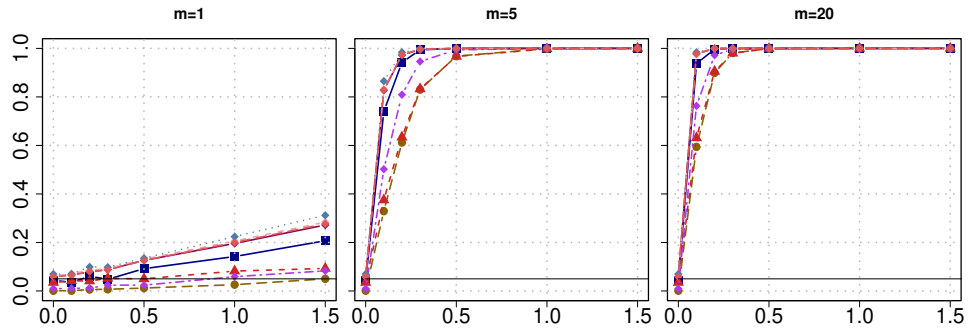


(c) *Setting 3*

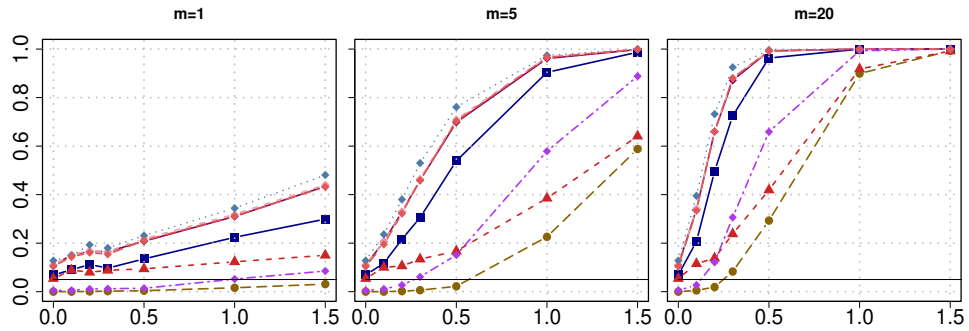
Figure S.8: Raw empirical rejection rates of the RP methods for various values of SNR in the x-axis. The RP method performs 200 random projections and applies different change point tests (CUSUM, Weighted, DE, HS, HR) and the Bonf combination method. The data-generating process follows (3.2) where the standard deviation σ_g follows Settings 1-3. The change point location is set at $\theta = 0.25$. The empirical rejection rate is based on 1000 simulations.



(a) *Setting 1*

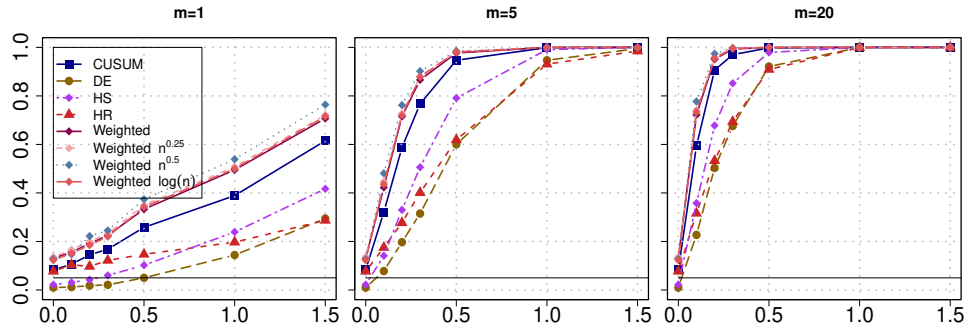


(b) *Setting 2*

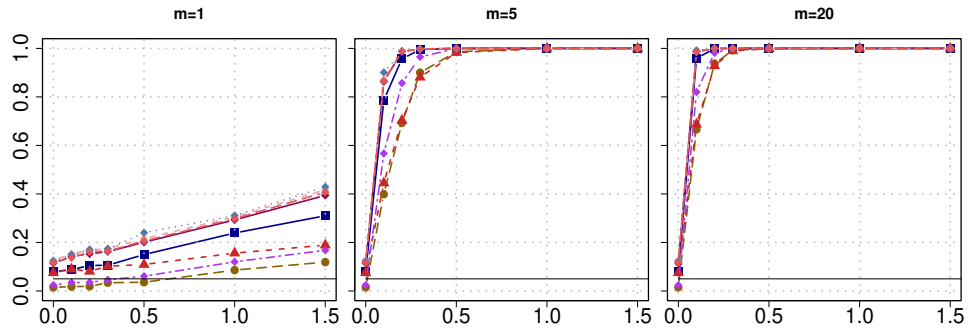


(c) *Setting 3*

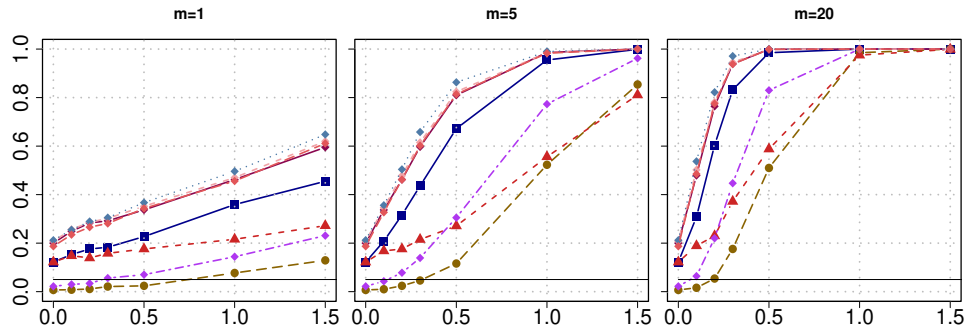
Figure S.9: Raw empirical rejection rates of the RP methods for various values of SNR in the x-axis. The RP method performs 200 random projections and applies different change point tests (CUSUM, Weighted, DE, HS, HR) and the BH combination method. The data-generating process follows (3.2) where the standard deviation σ_g follows Settings 1-3. The change point location is set at $\theta = 0.25$. The empirical rejection rate is based on 1000 simulations.



(a) Setting 1

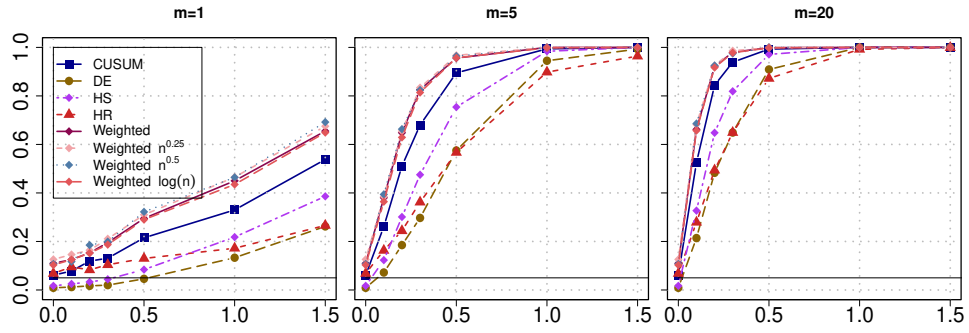


(b) Setting 2

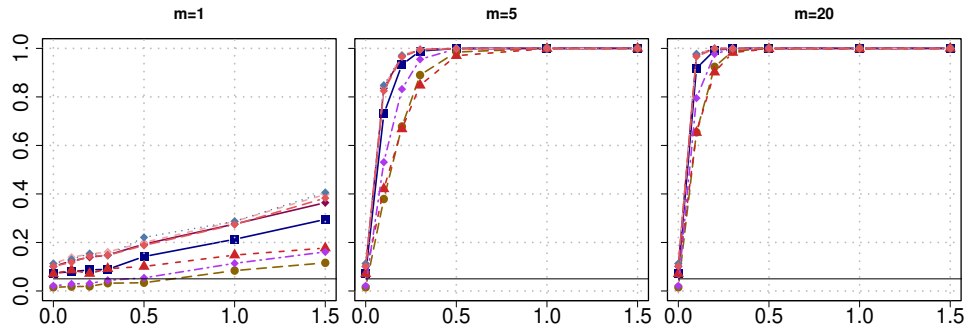


(c) Setting 3

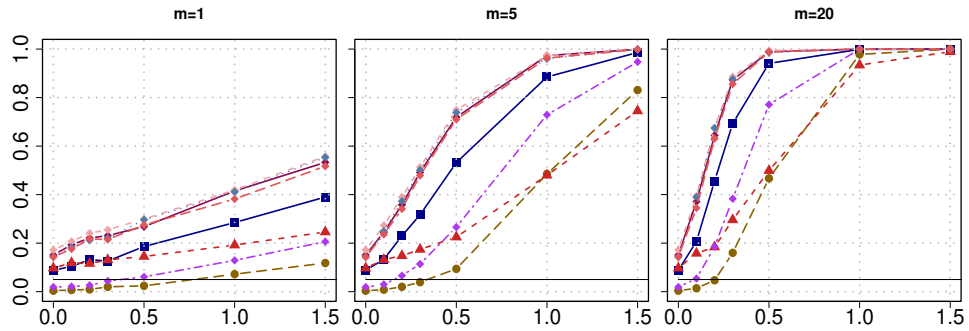
Figure S.10: Raw empirical rejection rates of the RP methods for various values of SNR in the x-axis. The RP method performs 200 random projections and applies different change point tests (CUSUM, Weighted, DE, HS, HR) and the HMP combination method. The data-generating process follows (3.2) where the standard deviation σ_g follows Settings 1-3. The change point location is set at $\theta = 0.25$. The empirical rejection rate is based on 1000 simulations.



(a) Setting 1

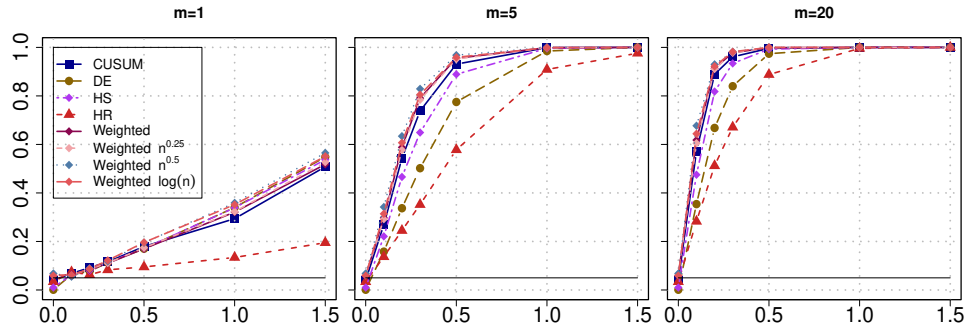


(b) Setting 2

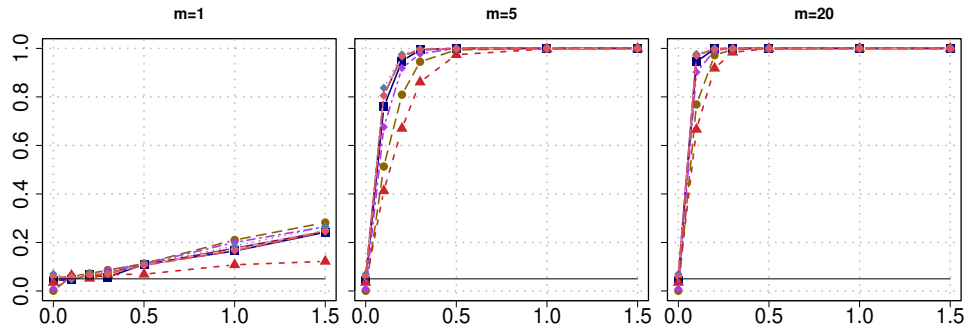


(c) Setting 3

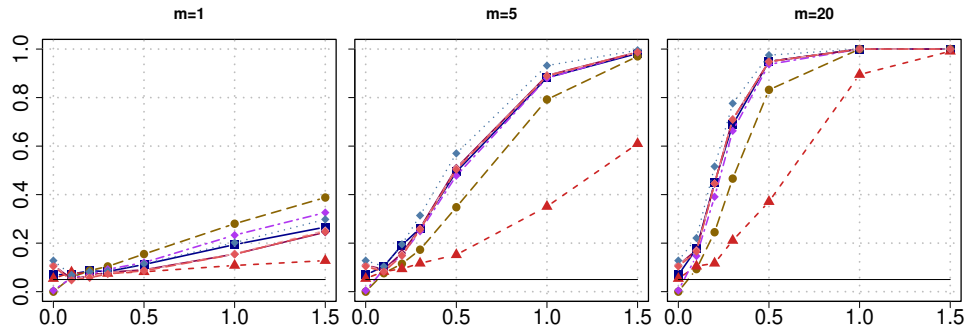
Figure S.11: Raw empirical rejection rates of the RP methods for various values of SNR in the x-axis. The RP method performs 200 random projections and applies different change point tests (CUSUM, Weighted, DE, HS, HR) and the CCT combination method. The data-generating process follows (3.2) where the standard deviation σ_g follows Settings 1-3. The change point location is set at $\theta = 0.25$. The empirical rejection rate is based on 1000 simulations.



(a) *Setting 1*

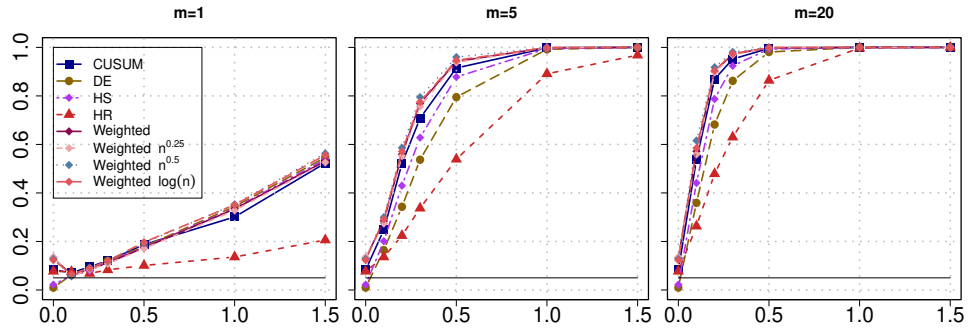


(b) *Setting 2*

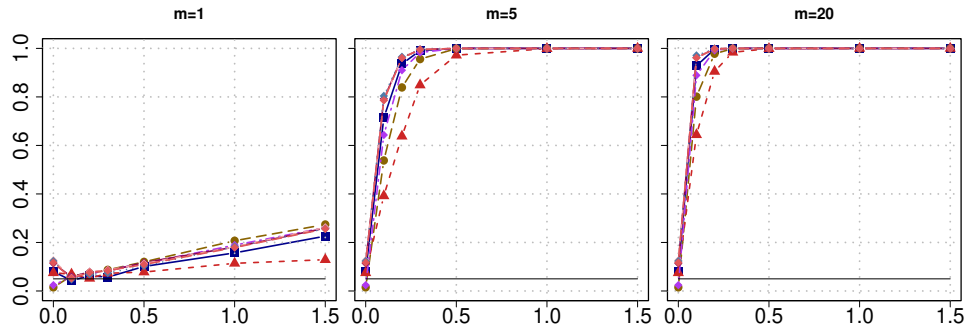


(c) *Setting 3*

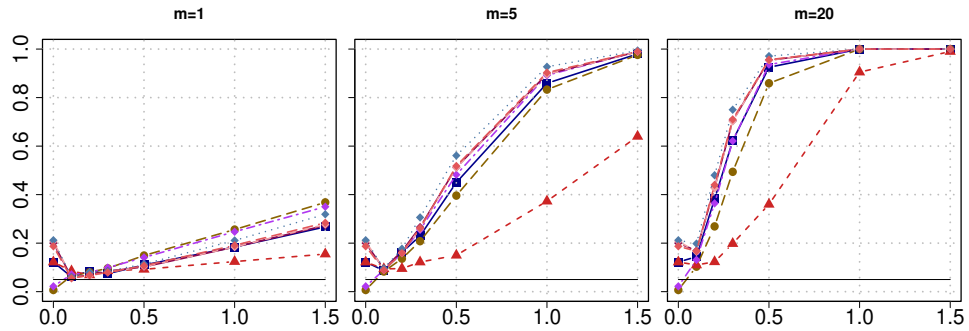
Figure S.12: Adjusted empirical rejection rates of the RP methods for various values of SNR in the x-axis. The RP method performs 200 random projections and applies different change point tests (CUSUM, Weighted, DE, HS, HR) and the BH combination method. The data-generating process follows (3.2) where the standard deviation σ_g follows Settings 1-3. The change point location is set at $\theta = 0.25$. The empirical rejection rate is based on 1000 simulations.



(a) *Setting 1*

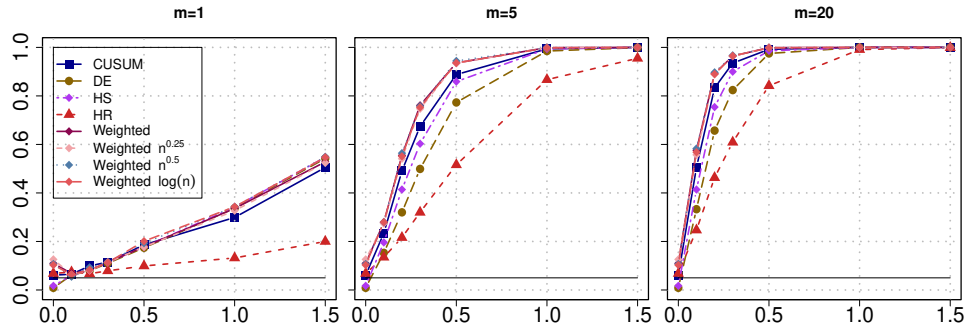


(b) *Setting 2*

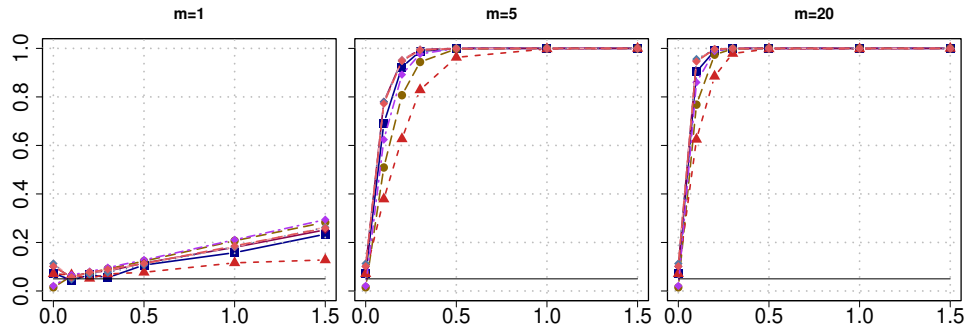


(c) *Setting 3*

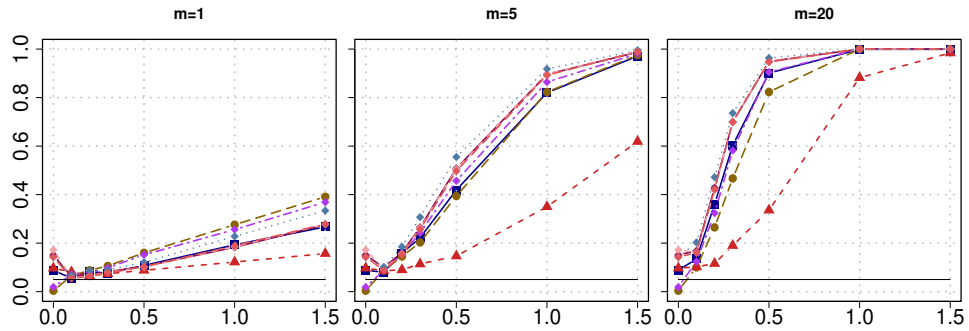
Figure S.13: Adjusted empirical rejection rates of the RP methods for various values of SNR in the x-axis. The RP method performs 200 random projections and applies different change point tests (CUSUM, Weighted, DE, HS, HR) and the HMP combination method. The data-generating process follows (3.2) where the standard deviation σ_g follows *Settings 1-3*. The change point location is set at $\theta = 0.25$. The empirical rejection rate is based on 1000 simulations.



(a) *Setting 1*

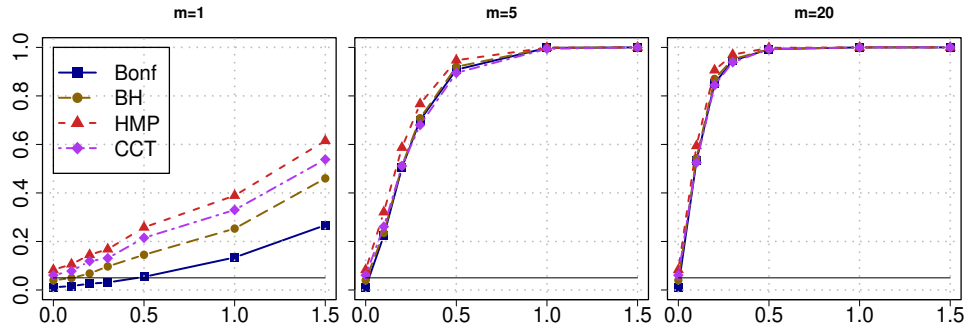


(b) *Setting 2*

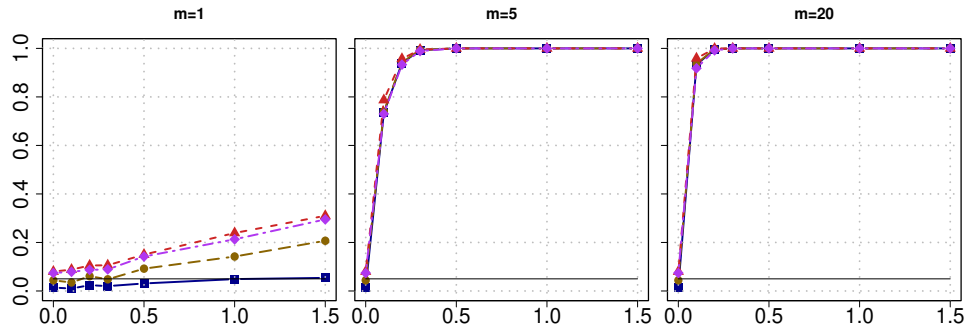


(c) *Setting 3*

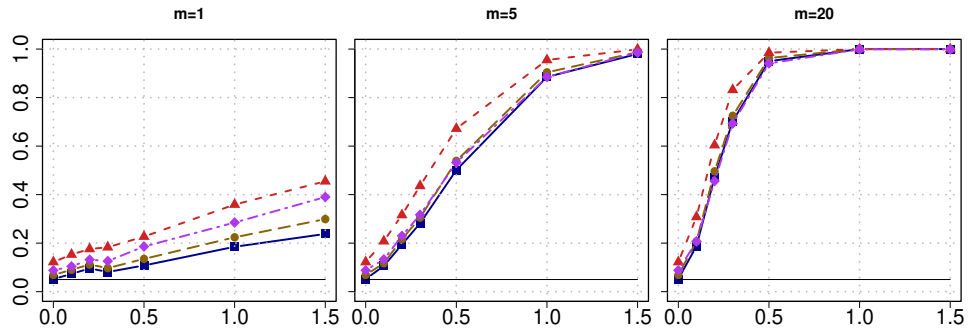
Figure S.14: Adjusted empirical rejection rates of the RP methods for various values of SNR in the x-axis. The RP method performs 200 random projections and applies different change point tests (CUSUM, Weighted, DE, HS, HR) and the CCT combination method. The data-generating process follows (3.2) where the standard deviation σ_g follows *Settings 1-3*. The change point location is set at $\theta = 0.25$. The empirical rejection rate is based on 1000 simulations.



(a) *Setting 1*



(b) *Setting 2*

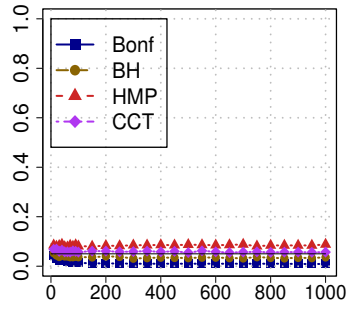


(c) *Setting 3*

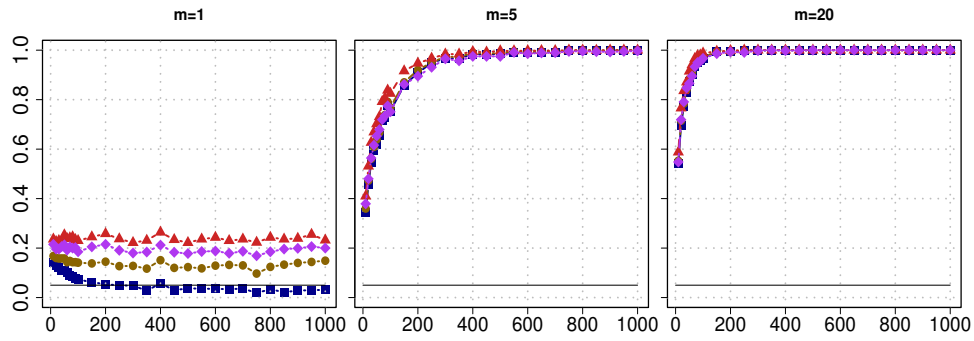
Figure S.15: Raw empirical rejection rates of the RP-Bonf, RP-BH, RP-HMP, and RP-CCT methods with the standard CUSUM test for various values of SNR in the x-axis. The RP method performs 200 random projections. The data-generating process follows (3.2) where the standard deviation σ_g follows Settings 1-3. The change point location is set at $\theta = 0.25$. The empirical rejection rate is based on 1000 simulations.

Empirical rejection rate under the null (significance level 0.05)					
		Bonf	HMP	BH	CCT
<i>Setting 1</i>	CUSUM	0.011	0.083	0.040	0.061
	DE	0.000	0.010	0.001	0.009
	HS	0.001	0.022	0.010	0.017
	HR	0.013	0.077	0.034	0.068
	Weighted	0.024	0.131	0.059	0.110
	Weighted $n^{0.25}$	0.024	0.136	0.065	0.126
	Weighted $n^{0.5}$	0.022	0.128	0.068	0.107
	Weighted $\log(n)$	0.021	0.123	0.059	0.103
<i>Setting 2</i>	CUSUM	0.014	0.080	0.044	0.074
	DE	0.000	0.015	0.001	0.015
	HS	0.000	0.024	0.009	0.021
	HR	0.017	0.075	0.035	0.071
	Weighted	0.025	0.114	0.060	0.101
	Weighted $n^{0.25}$	0.025	0.126	0.061	0.113
	Weighted $n^{0.5}$	0.027	0.123	0.070	0.113
	Weighted $\log(n)$	0.023	0.117	0.059	0.102
<i>Setting 3</i>	CUSUM	0.052	0.122	0.069	0.088
	DE	0.000	0.007	0.000	0.004
	HS	0.004	0.022	0.005	0.019
	HR	0.052	0.122	0.054	0.097
	Weighted	0.092	0.200	0.109	0.151
	Weighted $n^{0.25}$	0.086	0.208	0.108	0.172
	Weighted $n^{0.5}$	0.108	0.212	0.128	0.143
	Weighted $\log(n)$	0.083	0.187	0.104	0.143

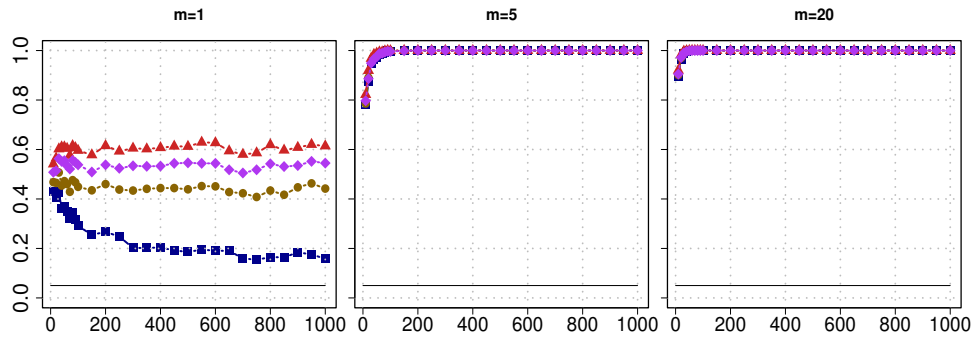
Table S.1: Empirical rejection rate under the null of RP method using different tests and p -value combination methods with $k = 200$.



(a) $SNR = 0$

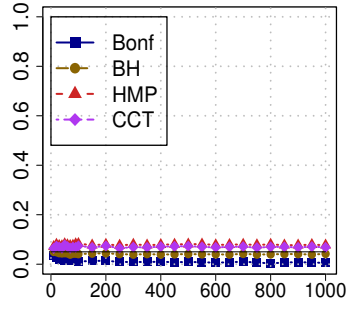


(b) $SNR = 0.5$

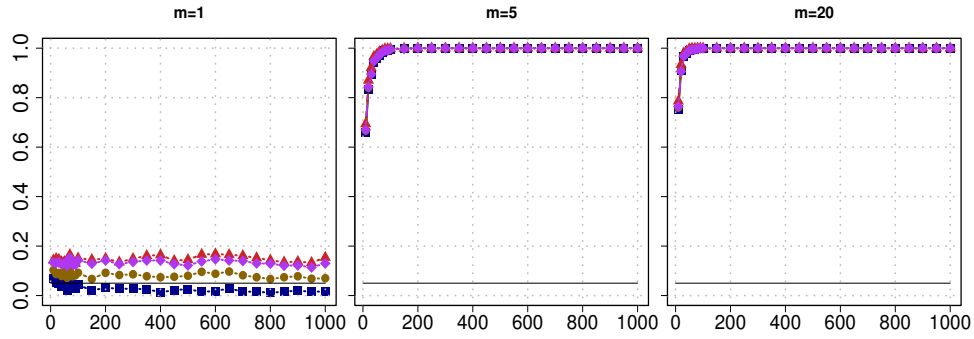


(c) $SNR = 1.5$

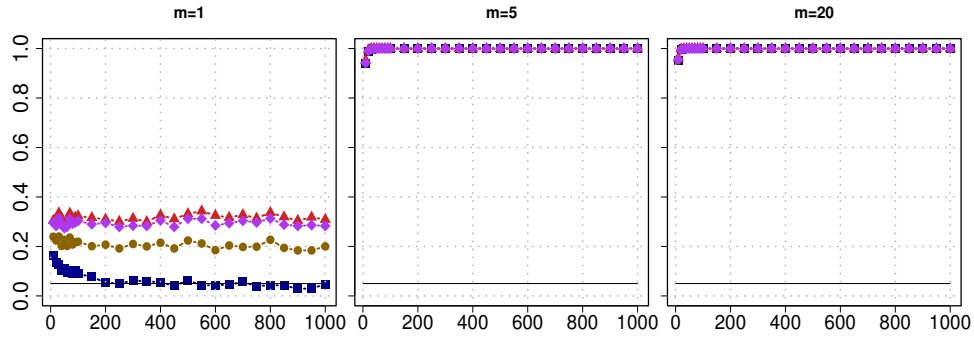
Figure S.16: Raw empirical rejection rates of the RP-Bonf, RP-BH, RP-HMP and RP-CCT methods with the standard CUSUM test for various choices of number k of random projections in the x -axis. The data-generating process follows (3.2) where the standard deviation σ_g follows *Setting 1*. The change point location is set at $\theta = 0.25$. The empirical rejection rate is based on 1000 simulations.



(a) $SNR = 0$



(b) $SNR = 0.5$



(c) $SNR = 1.5$

Figure S.17: Raw empirical rejection rates of the RP-Bonf, RP-BH, RP-HMP and RP-CCT methods with the standard CUSUM test for various choices of number k of random projections in the x -axis. The data-generating process follows (3.2) where the standard deviation σ_g follows *Setting 2*. The change point location is set at $\theta = 0.25$. The empirical rejection rate is based on 1000 simulations.

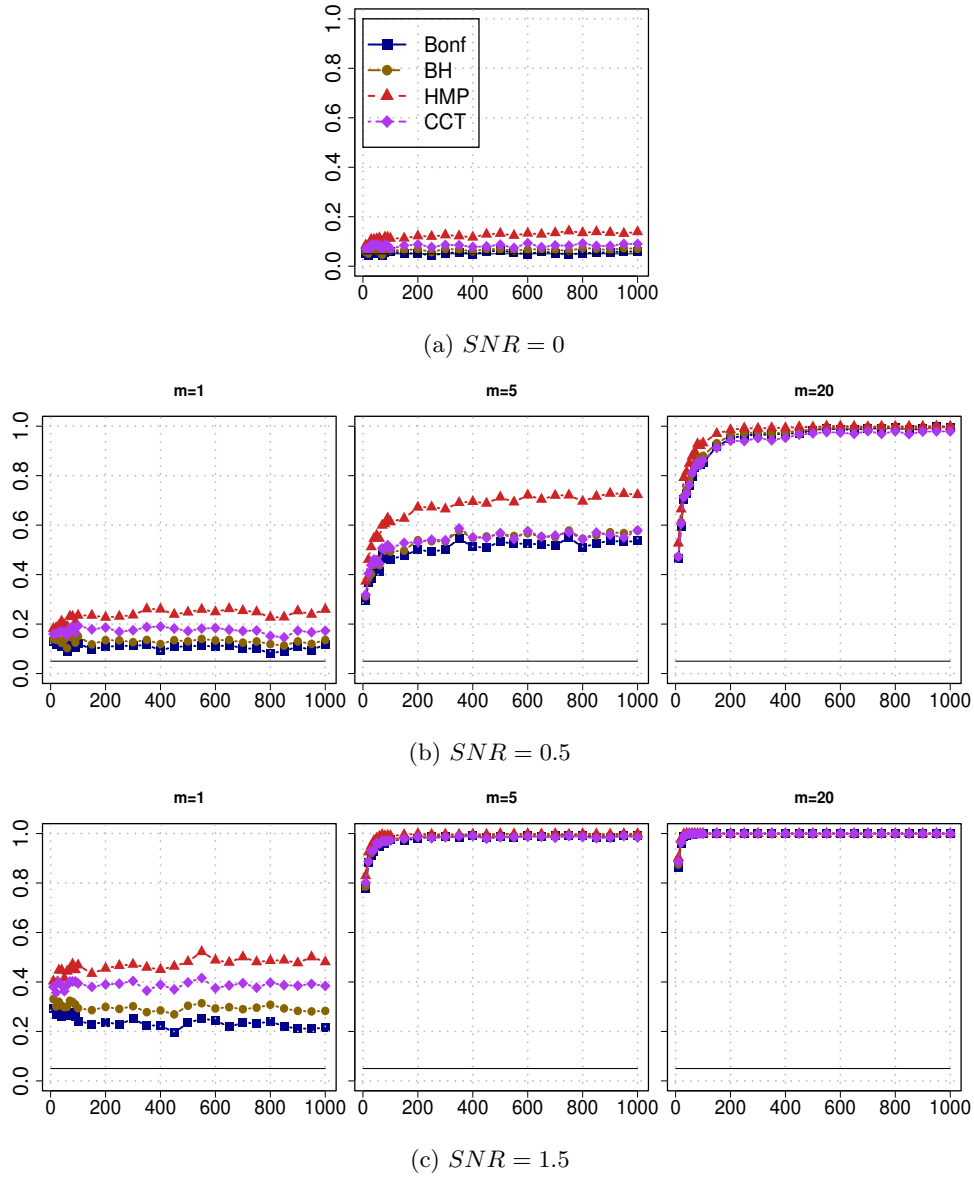
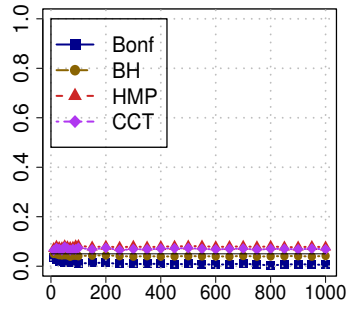
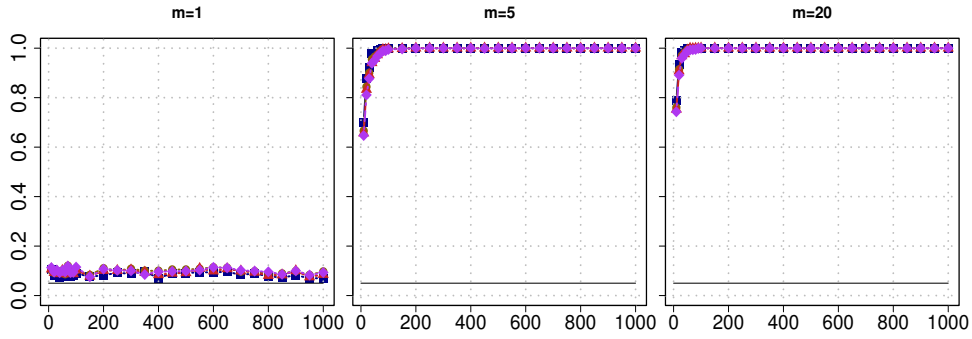


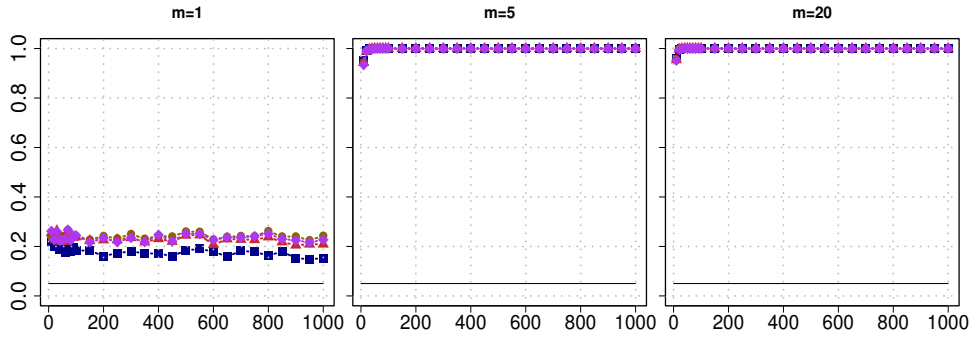
Figure S.18: Raw empirical rejection rates of the RP-Bonf, RP-BH, RP-HMP and RP-CCT methods with the standard CUSUM test for various choices of number k of random projections in the x -axis. The data-generating process follows (3.2) where the standard deviation σ_g follows *Setting 3*. The change point location is set at $\theta = 0.25$. The empirical rejection rate is based on 1000 simulations.



(a) $SNR = 0$

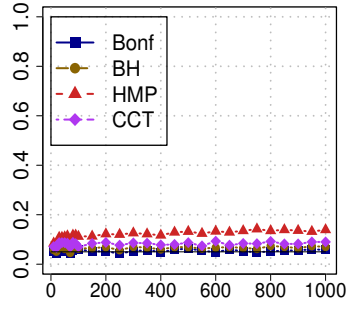


(b) $SNR = 0.5$

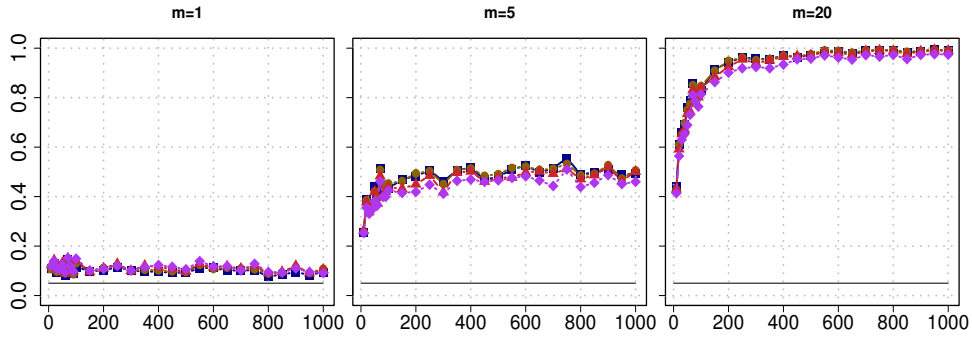


(c) $SNR = 1.5$

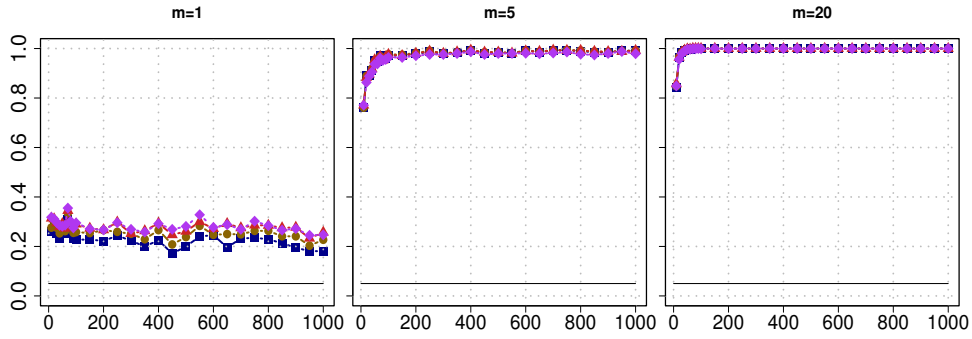
Figure S.19: Adjusted empirical rejection rates of the RP-Bonf, RP-BH, RP-HMP and RP-CCT methods with the standard CUSUM test for various choices of number k of random projections in the x-axis. The data-generating process follows (3.2) where the standard deviation σ_g follows *Setting 2*. The change point location is set at $\theta = 0.25$. The empirical rejection rate is based on 1000 simulations.



(a) $SNR = 0$

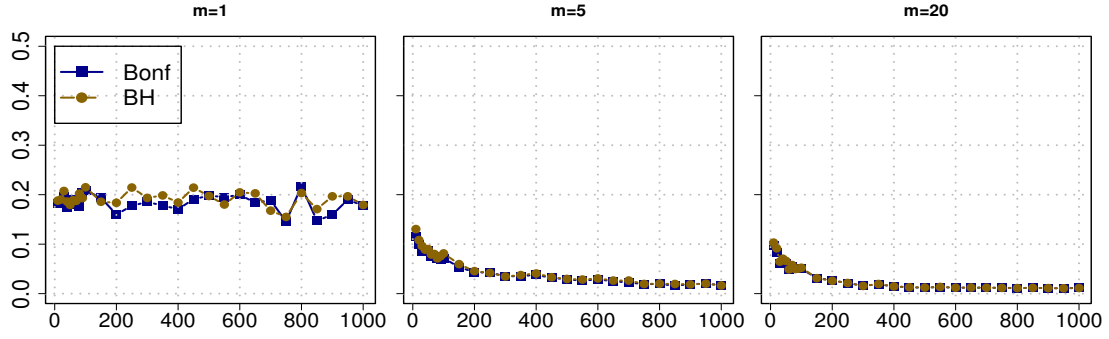


(b) $SNR = 0.5$

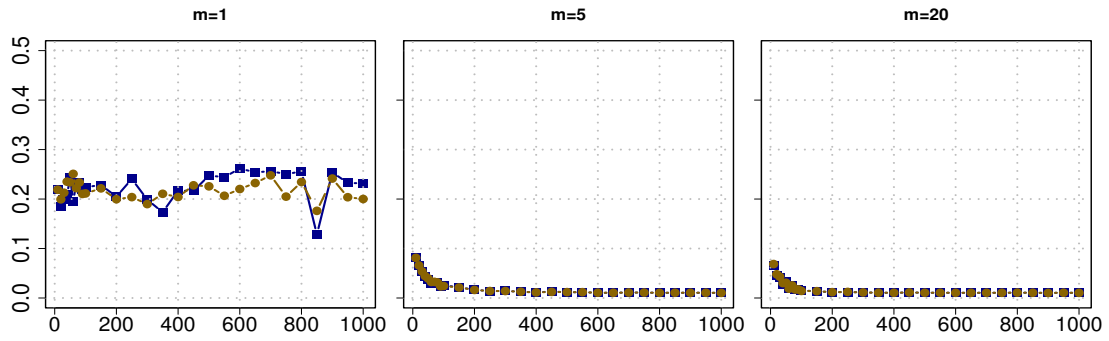


(c) $SNR = 1.5$

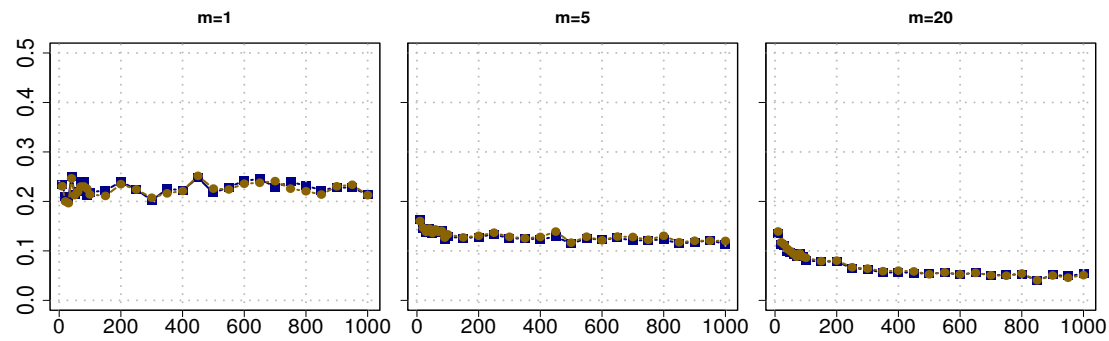
Figure S.20: Adjusted empirical rejection rates of the RP-Bonf, RP-BH, RP-HMP and RP-CCT methods with the standard CUSUM test for various choices of number k of random projections in the x-axis. The data-generating process follows (3.2) where the standard deviation σ_g follows *Setting 3*. The change point location is set at $\theta = 0.25$. The empirical rejection rate is based on 1000 simulations.



(a) Setting 1



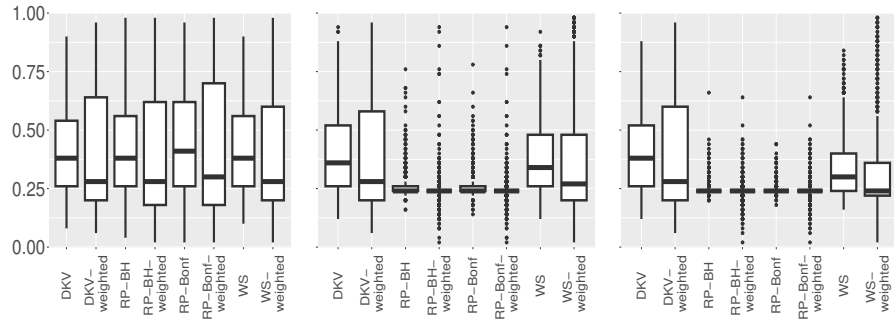
(b) Setting 2



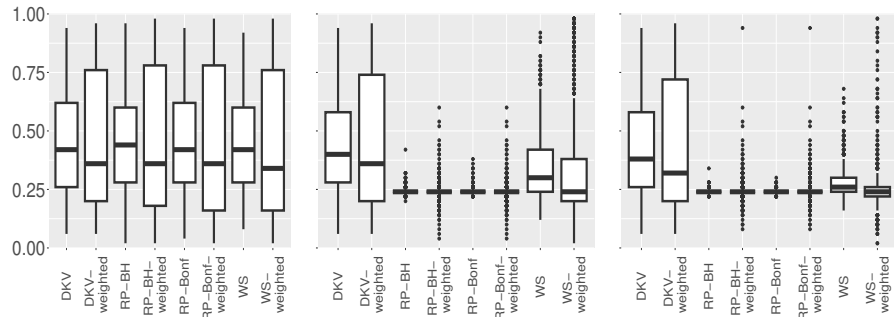
(c) Setting 3

Figure S.21: RMSE of estimated significant change point locations detected by the RP-Bonf and RP-BH methods with the standard CUSUM test for various choices of number k of random projections in the x-axis. The data-generating process follows (3.2) where the standard deviation σ_g follows Settings 1-3. The change point location is set at $\theta = 0.25$. The RMSE is based on 1000 simulations.

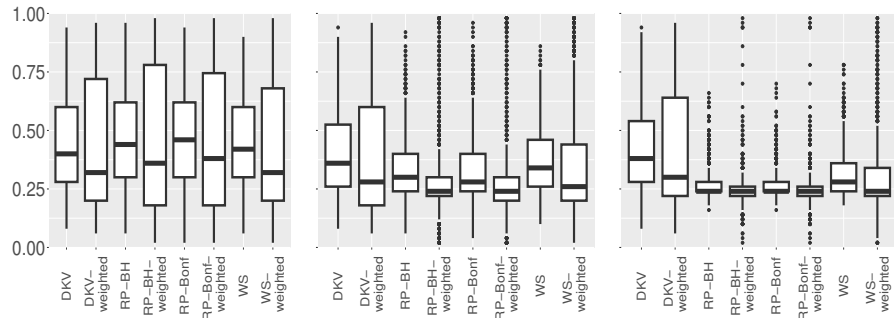
S.2 Comparison of different methods using weighted CUSUM



(a) *Setting 1*, with $m = 1, 5, 20$



(b) *Setting 2*, with $m = 1, 5, 20$



(c) *Setting 3*, with $m = 1, 5, 20$

Figure S.22: Estimated change point locations detected by different methods on 1000 simulations, using the standard CUSUM approaches or weighted CUSUM approaches with trimming choice of $\lfloor n\tau \rfloor = 1$. The data-generating process follows (3.2) where the standard deviation σ_g follows *Settings 1-3*. The change point location is set at $\theta = 0.25$. The magnitude of the break function is scaled by $SNR = 0.5$.

S.3 Repeating the procedure in Subsection 3.3 using additional datasets

This section presents additional simulation results for Subsection 3.3. Figures in this section are the same as Figure 7, except for the underlying dataset.

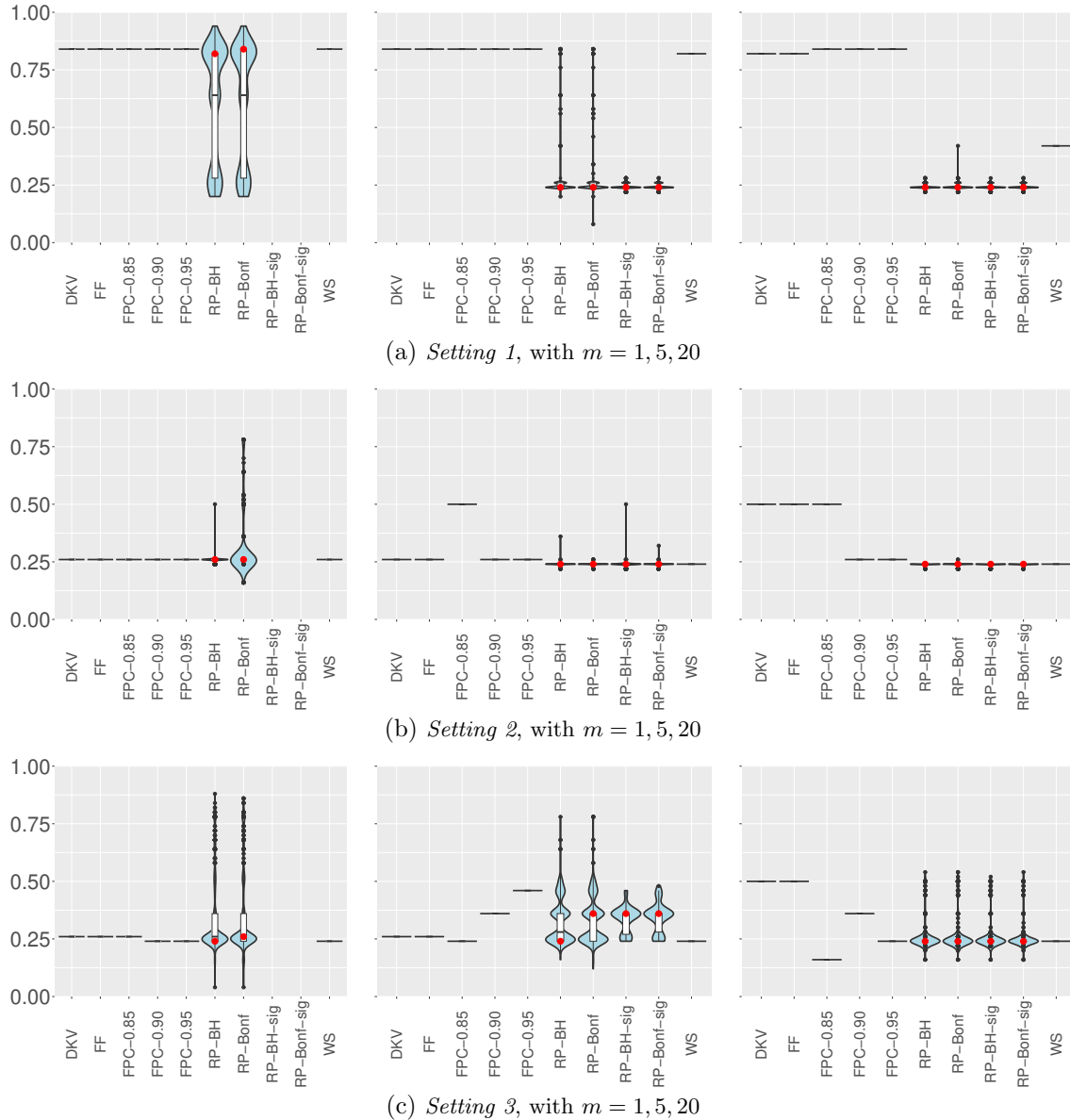


Figure S.23: Estimated change point locations detected by repeating the methods on one dataset (Dataset 1) 1000 times. For the RP methods, the mode of the estimated locations across the 1000 repetitions is marked by a red dot. The data-generating process follows (3.2) where the standard deviation σ_g follows Settings 1-3. The change point location is set at $\theta = 0.25$. The magnitude of the break function is scaled by $SNR = 0.5$.

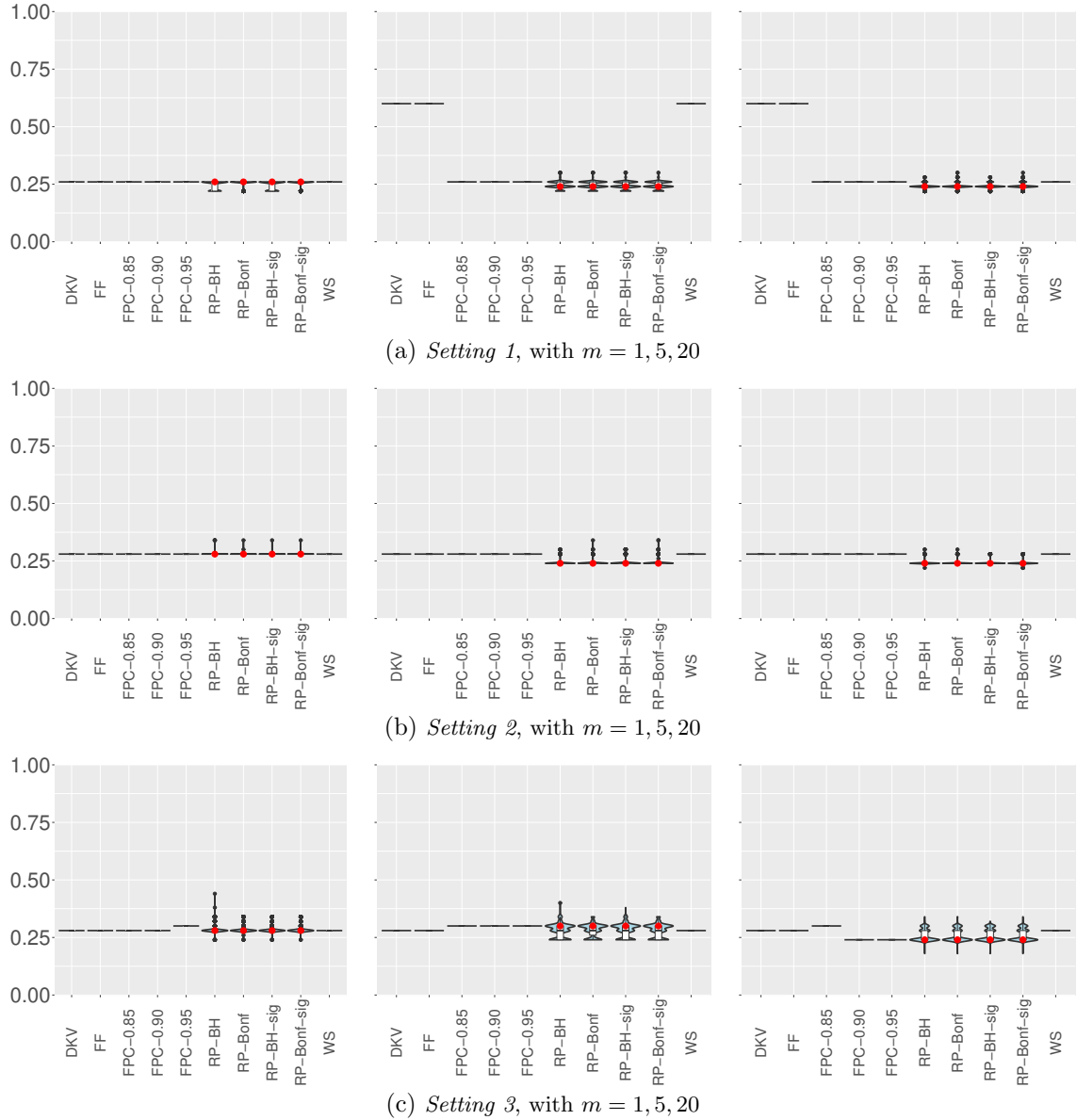


Figure S.24: Estimated change point locations detected by repeating the methods on one dataset (Dataset 2) 1000 times. For the RP methods, the mode of the estimated locations across the 1000 repetitions is marked by a red dot. The data-generating process follows (3.2) where the standard deviation σ_g follows *Settings 1-3*. The change point location is set at $\theta = 0.25$. The magnitude of the break function is scaled by $SNR = 0.5$.

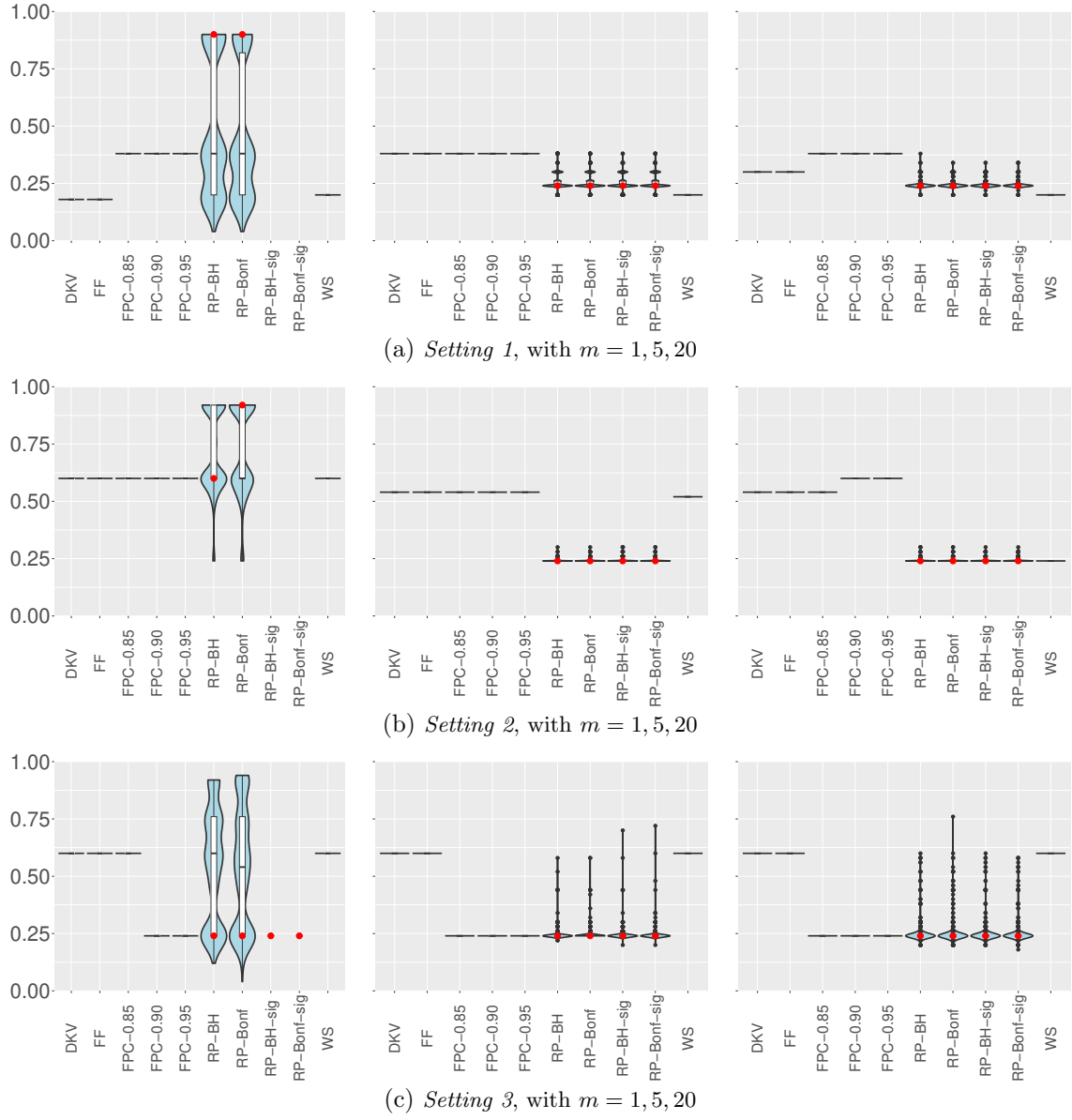


Figure S.25: Estimated change point locations detected by repeating the methods on one dataset (Dataset 3) 1000 times. For the RP methods, the mode of the estimated locations across the 1000 repetitions is marked by a red dot. The data-generating process follows (3.2) where the standard deviation σ_g follows *Settings 1-3*. The change point location is set at $\theta = 0.25$. The magnitude of the break function is scaled by $SNR = 0.5$.

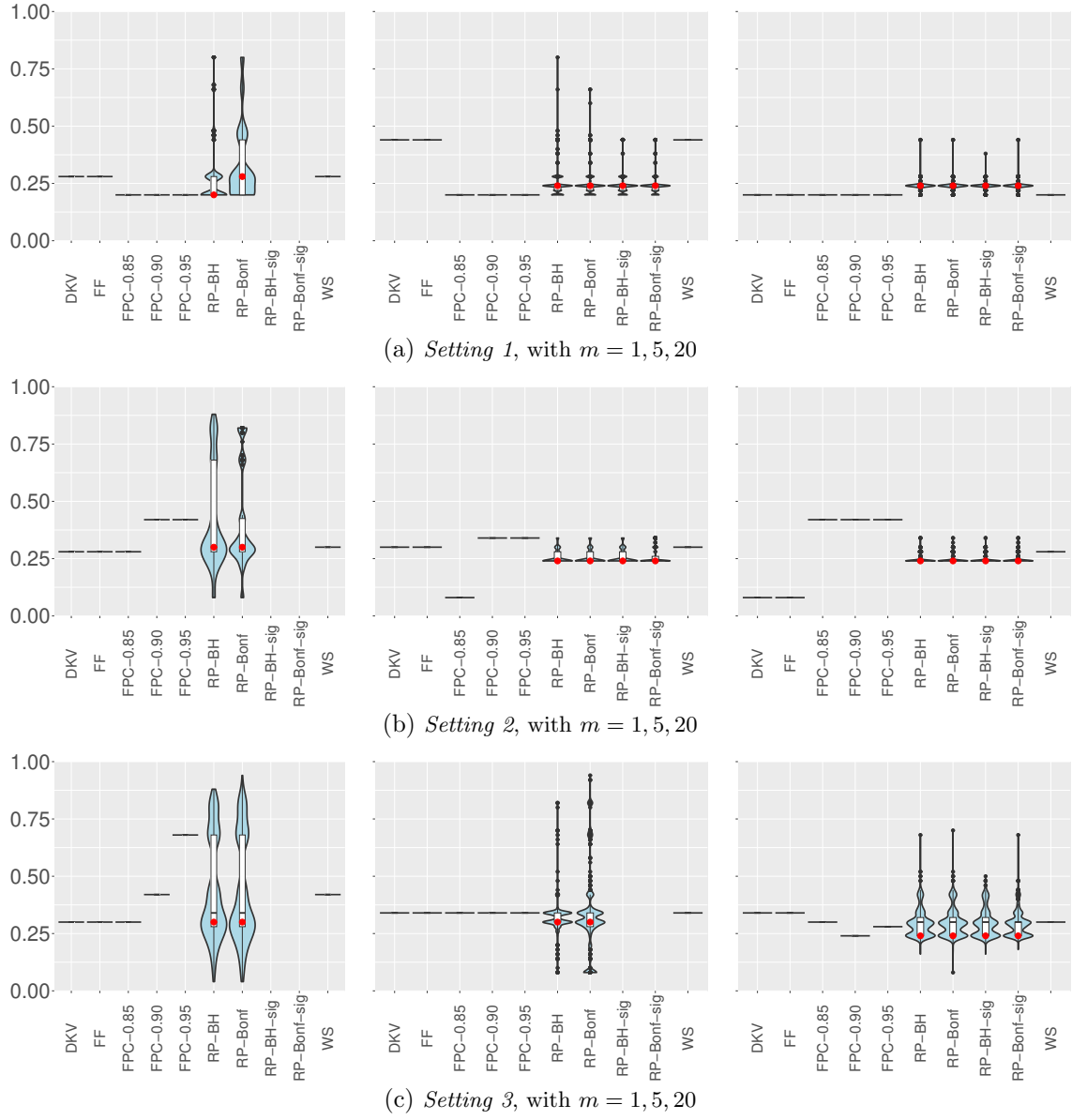


Figure S.26: Estimated change point locations detected by repeating the methods on one dataset (Dataset 4) 1000 times. For the RP methods, the mode of the estimated locations across the 1000 repetitions is marked by a red dot. The data-generating process follows (3.2) where the standard deviation σ_g follows Settings 1-3. The change point location is set at $\theta = 0.25$. The magnitude of the break function is scaled by $SNR = 0.5$.

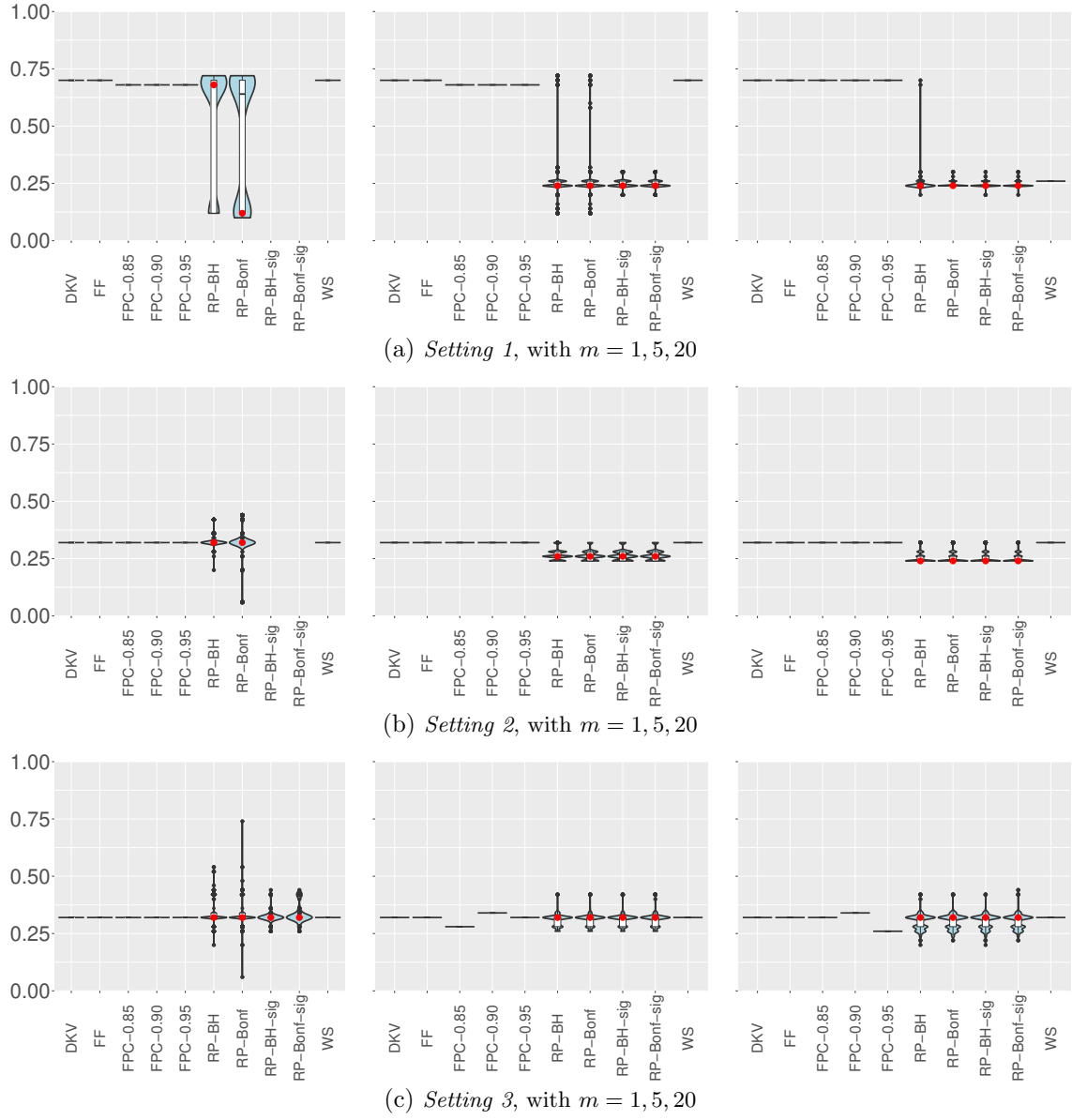


Figure S.27: Estimated change point locations detected by repeating the methods on one dataset (Dataset 5) 1000 times. For the RP methods, the mode of the estimated locations across the 1000 repetitions is marked by a red dot. The data-generating process follows (3.2) where the standard deviation σ_g follows Settings 1-3. The change point location is set at $\theta = 0.25$. The magnitude of the break function is scaled by $SNR = 0.5$.